Structure-function studies of MICAL, the unusual multidomain flavoenzyme involved in actin cytoskeleton dynamics.

Maria Antonietta Vanoni

Department of Biosciences
Università degli Studi di Milano
Via Celoria 26
20133 Milano, Italy
Phone: +390250314901; Fax: +390250314895; E-mail: maria.vanoni@unimi.it

Keywords:

MICAL; Flavoprotein; FAD-containing monooxygenase/oxidase; F-actin depolymerization; Semaphorin signaling; Cytoskeleton

Abstract

MICAL (from the Molecule Interacting with CasL) indicates a family of multidomain proteins conserved from insects to humans, which are increasingly attracting attention for their participation in the control of actin cytoskeleton dynamics, and, therefore, in the several related key processes in health and disease. MICAL is unique among actin binding proteins because it catalyzes a NADPH-dependent F-actin depolymerizing reaction. This unprecedented reaction is associated with its N-terminal FAD-containing domain that is structurally related to p-hydroxybenzoate hydroxylase, the prototype of aromatic monooxygenases, but catalyzes a strong NADPH oxidase activity in the free state. This review will focus on the known structural and functional properties of MICAL forms in order to provide an overview of the arguments supporting the current hypotheses on the possible mechanism of action of MICAL in the free and F-actin bound state, on the modulating effect of the CH, LIM, and C-terminal domains that follow the catalytic flavoprotein domain on the MICAL activities as well as that of small molecules and proteins interacting with MICAL.

Abbreviations

ABS, actin binding site; CasL, Crk (p38)-associated substrate-related protein; CC, coiled-coils; CH, calponin homology; CRMP, collapsin response mediator protein; DLS, dynamic light scattering; D-MICAL, *Drosophila melanogaster* MICAL; DTT, dithiothreitol; EHBP, Eps15 homology domain binding proteins; F-actin, filamentous actin; G-actin, globular actin; HRP, horseradish peroxidase; LIM, domain found in Lin11, Isl-1 and Mec-3 proteins; MALDI-TOF, matrix-assisted laser desorption ionization e time of flight mass spectrometry; MICAL, the Molecule Interacting with CasL; MICAL-cL, MICAL-like protein containing only the C-terminal domain; MICAL-L1, MICAL-L2, MICAL-like proteins 1 and 2; MO, monooxygenase-like domain; MOCH, truncated MICAL form comprising the MO and CH domains; MOCHLIM, truncated MICAL form comprising the MO, CH and LIM domains; MRTF-A , myocardin-related transcription factor-A; MS, mass spectrometry; MST, Ste20-like kinase; NDR, nuclear Dbf2-related; PAX5, paired box gene product 5; PHBH, p-hydroxybenzoate hydroxylase; pOHBz, p-hydroxybenzoate; PIP2, phosphatidylinositol bisphosphate; RBD, Rab binding domain; ROS, reactive oxygen species; SAXS, small-angle X-ray scattering; SDS, sodium dodecyl sulfate; SH3, Src homology domain-3; SRF, serum response factor .

Highlights

- MICAL is a multidomain flavoenzyme participating in actin cytoskeleton dynamics
- The key role of MICAL in fundamental processes is being increasingly demonstrated
- It catalyzes NADPH-dependent oxidase and F-actin depolymerizing reactions
- Hypotheses on the mechanism of MICAL's reactions are critically discussed
- How MICAL may be modulated by its domains and interacting proteins is also reviewed

Introduction

MICAL indicates a family of multidomain, mainly cytoplasmic, proteins, which participate in the control of actin cytoskeleton dynamics thanks to the unprecedented NADPH-dependent F-actin depolymerizing reaction associated with their N-terminal FAD-containing domain. The additional calponin homology (CH), LIM (from Lin-11, Isl-1 and Mec-3 gene products) and C-terminal regions, which are typical protein interaction domains, play modulatory roles.

Since their discovery in 2002 [1, 2], a great deal of work has focused on MICALs biological function and regulation by combining genetic and cell biology approaches on model organisms and selected cell lines. The structural features of several isolated domains have been established. Several studies aimed to determine the catalytic properties of MICALs, especially the mechanism of the F-actin depolymerizing activity, as well as their modulation by the additional domains and interacting proteins.

In this article, knowledge on the biological function of MICAL proteins and its possible implications in disease will be summarized. Next, structural information on MICALs will be briefly reviewed to provide a framework for the discussion of MICALs catalytic activities and their regulation, which will be the focus of this article. Due to the vast literature related to the topic, it will not – unfortunately - be possible to quote all relevant work.

MICAL stands for the Molecule Interacting with CasL from the discovery of the first member of the family (MICAL-1) as an interactor of CasL in a human thymus library [1]. CasL (from Crk-associated substrate-related protein lymphocyte type) is also known as NEDD9 (from neural precursor cell expressed, developmentally down-regulated 9) or HEF1 (from human enhancer of filamentation 1) [3, 4]. It is a docking protein involved in signaling pathways related to T-cell differentiation, cell-cell junctions formation, cell migration in part in response to integrin activation and it is also associated with several cancer forms [4-6]. Shortly after the first report on MICAL-1 [1], studies in *Drosophila melanogaster* revealed that MICAL is a plexin interactor and participates in axon steering by mediating the repulsive signaling of extracellular semaphorins [2].

Correct axon navigation during development is under the control of a complex network of attractive and repulsive signals [7]. Among them are semaphorins, which form a broad family of membrane-bound and secreted proteins [8-11]. They have been originally discovered as repulsive cues in the axon growth process, but are now implicated in a variety of other processes related to cell proliferation, migration and differentiation not only in the nervous tissue, such as, e.g.: angiogenesis, cardiogenesis, immune cell differentiation and bone morphology [12-19]. In a simplified scheme to illustrate semaphorin action, binding of semaphorin to their plexin receptors on the axon growth cone determines recruitment and activation of a number of proteins, including small GTPases, the collapsin response mediator proteins (CRMP) and, as a novel member, MICAL. As a result, local disassembly of the actin cytoskeleton takes place with axon growth cone retraction, which is followed by regrowth upon the combined action of attractive and repulsive stimuli [11, 20-24].

The initial studies also led to identify only one gene encoding MICAL in drosophila, but three genes coding for MICAL-1, -2 and -3 in vertebrates [1, 2, 25-28]. MICAL-like proteins (MICAL-L1 and MICAL-L2), encoded by different genes, also exist [28, 29]. They also participate in actin cytoskeleton dynamics, but they lack the N-terminal flavoprotein domain so that their function is independent from NADPH-dependent oxidoreduction reactions. Whether some of their biological roles overlap with those of MICALs is not clear, but they seem mainly involved in endocytic recycling [29-31]. While it has been shown that semaphorin 3A activates MICAL-1 through its PlexinA receptor, it is not fully clear if all other MICAL forms respond to semaphorin-plexin interaction. Regulating pathways independent from semaphorins may also be operative for all MICALs as shown by the interaction between MICAL and MICAL-like forms with proteins of the Rab family [25, 26, 29, 31-39], guanidine exchange factors [40], beside the possible modulatory roles of CasL [1], CRMP [41, 42] and other proteins [43].

The fundamental finding that MICAL is essential for the transduction of semaphorin signaling in drosophila [2], thus, for the correct development of neurons, stimulated a series of studies that extended the role of MICALs to a wide range of processes requiring actin filaments dynamics, such as, e.g., formation of tight junctions, synapses and the organization of myofilaments (drosophila MICAL, [27]), dendrite pruning (MICAL-1, [44, 45]), vesicle trafficking (MICAL-3, [33]), gene expression regulation (MICAL-2, [46]). Very recently, it has been shown that MICAL-1 is essential to complete cell division [32]. Reports that MICAL or MICAL-like proteins are involved in host defense from pathogen infection or infectivity have also appeared [47, 48]. It remains to be established if and how MICALs participate in the control of microtubules and intermediate filaments as suggested by its interaction with CRMP [21, 41, 42] and vimentin [1], respectively.

Some of MICAL roles may not be related to its oxidoreductase activity as suggested for the anti-apoptotic function of MICAL-1. In this role it sequesters the nuclear Dbf2-related kinase (NDR1/2, [23, 43, 49]). Thus, it antagonizes MST1-induced NDR activation and, therefore, interrupts the apoptotic signal of MST (Ste-20-like kinase). The interaction with CasL has also been proposed to sequester this protein from the integrin-dependent pathway [1], but the observation has not been apparently followed up by further specific studies.

Modulating MICALs function has been proposed to be beneficial to prevent or treat a broad range of diseases only in part paralleling the aim to interfere with semaphorin signaling, which are emerging as important therapeutic targets [9, 11, 50-52] . MICAL-2 isoforms found in prostate cancer cells have indicated a role of MICAL in tumor progression [53]. Unfortunately, the accession codes for such MICAL-2 prostate variants (PV1, AB126828 and PV2, AB126829) appear to lead to the same nucleotide sequence that seems to encode a human protein unrelated to MICAL (BEN domain-containing protein 4 isoform a , NP_997289, 534 aa; http://smart.embl.de/smart/do_annotation.pl?DOMAIN=SM01025).

However, increased expression of MICAL-2 was associated with the epithelial to mesenchimal transition in gastric and renal tumors that leads to metastasis formation, the cause of most of cancer-related deaths [54]. MICAL-1 seems to be associated with melanoma [49], but in a manner related to its anti-apoptotic role as a binder of NDR1/2 [43], while its contribution to the generation of oxidative stress was shown to be important

for invasiveness of breast cancer cells [55]. Down-regulating MICAL's expression decreased the invasiveness phenotype of the cancer cells [54, 55]. MICALs may contribute to scar formation following spinal cord injury and modulation of its activity has been proposed to beneficial for the treatment of neuronal degeneration [56, 57]. Altered levels of MICAL have even been associated with epilepsy [58].

A thorough analysis of the wealth of information from genome sequencing and expression profiling seems missing, but it could be useful to clarify the correlation between specific mutations and the expression levels of MICAL (iso)forms with tissues distribution, developmental stage and disease. MICALs are expressed in most tissues with only partially overlapping patterns indicating that they all play roles in cellular plasticity, but may have different specific roles [19, 20, 23, 56, 59, 60]. In this respect, the function of drosophila MICAL in dendrite pruning was shown to be controlled by SOX14, which responds to ecdysone [44]. Correct splicing of drosophila MICAL appears to require a functional ubiquitin-proteasome system, suggesting that a similar mechanism is operative in vertebrates [45]. Human MICAL-3 expression was reported to be under the control of PAX5 (from Paired Box Gene 5 product) and binding motifs for several other transcription factors have been found upstream one of its potential [61] promoters. Interesting its pre-mRNA embeds microRNA648 that target endothelin-1 whose elevated levels induce pulmonary hypertension in sickle cell anemia [61], further increasing the interest in MICAL, but also further complicating the dissection of its biological roles.

In this complex scenario, a contribution to the understanding of MICALs comes from *in vitro* structure-function studies on isolated native and engineered protein forms.

MICAL architecture: an overview.

Sequence analyses revealed that the three MICAL forms (MICAL-1, -2 and -3) in vertebrates and the single MICAL form of the drosophila model organism are multidomain proteins. They are very similar to each other with respect to the sequence of the flavoprotein, CH and LIM domains, while the interdomain segments and sequences of the C-terminal regions are less conserved. Since detailed sequence comparisons have already been presented by us (Figure 4, [62]), only a schematic distribution of (sub)domains and fingerprints is shown here (Figure 1A) with details of representative protein sequences given as appropriate.

All MICALs contain a conserved N-terminal region with sequence similarities with FAD-dependent enzymes of the oxidase/monooxygenase families (residues 1 – 489 of human MICAL-1, Figure 1). Determination of the three-dimensional structure of the mouse MICAL-1 N-terminal flavoprotein domain [63, 64] showed that it is similar to p-hydroxybenzoate hydroxylase (PHBH), the prototype of class A monooxygenases [65-68]. For this reason, the N-terminal flavoprotein domain will be indicated as MICAL-MO, or MO from monooxygenase-like domain, instead of "redox", "FAD", and even "EN" used in other publications. This convenient acronym is not meant to imply that a hydroxylating reaction is actually catalyzed, as discussed below.

In MICAL-1 the MO domain is followed by the calponin homology (CH, residues ~510-613 for human MICAL-1) and the LIM domain (residues ~688-756, Figure 1). The C-terminal region contains a PPKP Pro-rich motif for the interaction with the Src Homology 3 (SH3) domain of CasL ([1], residues 830-833 for human MICAL-1) and a Glu-rich region (residues ~866-880 for human MICAL-1) of unknown function. The regions predicted to form coiled-coils (CC) at the C-terminus (residues 918-1067) has now been shown to consist of three α-helices forming a rather flat surface and to serve for Rab binding [32, 69]. The C-terminal region is believed to be the site, which is mainly responsible of the interaction of MICAL with several other proteins (e.g.: PlexA [2], vimentin [1], NDR1/2 [43], CRMP [41]).

In MICAL-3 the LIM domain is conserved although it is separated from the CH domain by a protein fragment longer than the equivalent region in MICAL-1. In the C-terminal region, the Pro-rich region is conserved. A Glu-rich region is more extended than that of MICAL-1 (residues 910-1052) and the similarity is low. The motifs for the formation of CC are present, and they have also been shown to form the Rab binding domain [69]. The peptides connecting these potentially functional regions are longer than in MICAL-1. A bipartite RKRX(14) KRRK sequence (residues 663-683 of human MICAL-3) has been proposed to be a nuclear localization signal [46] conserved in MICAL-2 (see below). In MICAL-1 only a RSR motif is found at position 644-646. Accordingly, MICAL-3 was found in the nucleus of HEK293T along with MICAL-2 but not MICAL-1 [46]. However, MICAL-3 is also found in the cytoplasm where it may form complexes with Rab proteins [33] so that for this and the other MICAL forms the precise localization (or re-localization) in cell compartments still needs to be determined.

MICAL-2 is similar in length to MICAL-1, but it differs from both MICAL-1 and MICAL-3 for the lack of the C-terminal region. The LIM domain is at the C-terminus of the protein, well separated from the CH domain. Motifs that may allow the formation of coiled-coils (or α-helices) have been found in the protein segment between the CH and LIM domains (residues 837 – 971 of human MICAL-2, [62]) but also in the 1070-1124 region that follows the LIM domain. This region may be responsible of the binding of Rab1 detected also for MICAL-2 [25, 26]. A PSPP motif, conserved within the MICAL-2 proteins (residues 899 – 902 for the human species) may correspond to the PXXP motif that was identified as the SH3 domain binding site in MICAL-1 and MICAL-3. A RKRX(14)KRRRK bipartite nuclear localization signal was also found at position 660-681 of human MICAL-2 [46]. Accordingly, MICAL-2 partially localizes in the nucleus of HEK293T, COS7 and HeLa cells where it determines the nuclear actin levels and, as a consequence, modulates the transcription of genes (mainly involved in cell differentiation and motility) under the control of the serum response factor (SRF)/myocardin-related transcription factor-A (MRTF-A) complex [46].

Drosophila MICAL is much longer than vertebrate MICAL-1, -2 and -3 due to the different length of the poorly conserved interdomain regions. Its overall architecture is similar to that of MICAL-1 and MICAL-3, but it apparently lacks the Glu-rich region between the Pro-rich peptide and the C-terminus where motifs for CC formation are located.

General properties of purified MICAL preparations for *in vitro* studies.

Various MICAL forms have been produced and purified in several laboratories for *in vitro* studies. Only in a few cases the preparations have been characterized in sufficient detail to provide a set of reference information on quality and general properties of the protein preparations across full-length and truncated forms and various laboratories.

Early on, the mouse MICAL-1 MO domain has been produced in *Escherichia coli* by two laboratories that determined its structure [63, 64] revealing the similarity with PHBH. The mouse MICAL-1 MO was also used to demonstrate that this protein catalyzes a hydrogen peroxide-producing NADPH oxidase activity ([63], see below). Drosophila MICAL forms comprising the MO domain (MICAL-MO or just MO) and both the MO and CH domains (MICAL-MOCH or MOCH) have been produced in *E. coli* and purified to study their NADPH-dependent F-actin depolymerizing activity [70-73]. However, it was only recently that lab protocols have been presented [74]. Mouse MICAL-1, and MICAL-2 MO and MOCH forms have been produced to study their *in vitro* actin depolymerizing activity [46, 75]. The structure of mouse MICAL-1 MOCH has been recently presented [76] along with mechanistic information (see below). The CH and LIM domains of human MICAL forms have been isolated to determine their structures by NMR. Recently, various forms of the C-terminal regions of human MICAL-1 and -3 have been produced for the determination of their three-dimensional structure and to study their complexes with Rab proteins [32, 69]. The mouse MICAL-2 MO has also been produced in *E. coli* and characterized [77].

The production and basic characterization of the full-length form of human MICAL-1, as well as of the progressively truncated variants lacking the C-terminal region (MOCHLIM), the LIM (MOCH) and the CH domain (MO) have provided a set of methods for the study of this class of enzymes and benchmark information [78, 79].

The human MICAL-1 forms were produced in *E. coli* cells [78, 79], like all other MICAL species. They are purified by combining metal-chelate, ion exchange and gel filtration chromatographies in quantities that now reach at least 0.5 mg/g of starting cell paste. Variations of similar protocols were successful for the production and purification of MICAL forms from different organisms (see above). The protein yield is similar to that reported for mouse MICAL-1 and MICAL-2 MO, but significantly higher than that reported for drosophila MOCH (2 mg from 45 g cells, [74]). The human MICAL-1 forms exhibit the yellow, orange or brownish color often reported for MICALs containing the MO domain (e.g.: [74, 77]). Accordingly, the absorption spectrum in the visible region (Figure 2) shows an absorption band at wavelength greater than 500 nm, which may be attributed to the charge-transfer complex between FAD and Trp400 (Trp405 for MICAL2, [62]) observed in the mouse MICAL-1 MO crystal structures [63, 64], rather than the fact that "the protein backbone shields the FAD from absorbing light" as stated in [74].

MICAL forms readily release the FAD coenzyme upon guanidine-, heat- or SDS-denaturation allowing for the determination of the extinction coefficient and stoichiometry of bound FAD. SDS-treatment offers the advantage of maintaining the denatured protein in solution [80], so that the removal of denatured protein by centrifugation described in [74] is not needed nor actually possible.

Extinction coefficients at 458 nm of 8.1 – 8.9 $mM^{-1}cm^{-1}$ have been reported for human MICAL-1 forms [78, 79], and drosophila MICAL-MOCH [74]. The extinction coefficient of mouse MICAL-2 MO was slightly higher (9.8 mM^{-1}cm-1, [77]) and the absorption maximum was at a lower wavelength (445 nm *versus* 458 nm). For practical purposes a common extinction coefficient at 458 nm of 8.1 $mM^{-1}cm^{-1}$ is used for all human MICAL-1 forms [78, 79]. Results consistent with the presence of 1 FAD and two Zn^{++} ions per protein molecule were obtained for all human MICAL-1 forms and for the MOCHLIM and full-length MICAL, respectively. Drosophila MICAL MOCH was reported to be isolated with precisely 1 mol FAD bound per protein molecule [74]. However, in this case protein concentration was determined from the absorbance at 280 nm and the extinction coefficient calculated for the apoprotein, which leads to overestimating MICAL concentration (see below).

Determination of the stoichiometries of FAD bound to all forms of MICAL and of zinc ions bound to forms containing the LIM domain, as well as the calculation of turnover numbers, require an accurate determination of protein concentration. The use of the extinction coefficient at 280 nm calculated from the protein sequence with programs like the Protparam tool of the Expasy suite (http://web.expasy.org/cgi-bin/protparam/protparam, [81]), which ignore the absorbance of the FAD coenzyme in the UV (see, e.g.: [74, 76]) may lead to overestimating the concentration MICAL forms by up to 30% (see comments in [81, 82]). In Table 1 the extinction coefficients experimentally determined for human MICAL-1 forms at 458 nm are shown along with those calculated at 280 nm by adding the value obtained for the apoprotein and the extinction coefficient of FAD at 280 nm in diluted buffer at pH 7 (21 $mM^{-1}cm^{-1}$). The corresponding values of the guanidine-denatured protein species are also shown with the extinction coefficient of FAD at 280 nm calculated experimentally as 22. 7 $mM^{-1}cm^{-1}$.

Human and mouse MICAL-1 MO and MOCH are monomeric in solution [63, 64, 76, 78, 79]. Accordingly, the CH domain of human MICAL-1 was monomeric [83, 84]. Human MOCHLIM behaves as a dimer at low protein concentration (0.5 mg/ml), but it tends to oligomerize at higher concentrations (Vitali and Vanoni, unpublished). Full-length human MICAL-1 seems to exist in solution as a mixture of compact monomers and dimers, as judged by combining analytical gel filtration, dynamic light scattering and small angle X-ray scattering (unpublished). Whether this property is biologically significant and is related to the presence of the LIM and/or of the C-terminal region still needs to be determined (see also below). The helical region at the very C-terminus of MICAL-1 is monomeric both in solution and in the crystal structure [32, 69]. On the contrary, the corresponding part of MICAL-3 forms dimers as described in the next section [69].

Structural information on MICALs.

The structure of mouse MICAL-1 MO was presented in two independent back-to-back papers in 2005 ([63, 64], Table 2, Figure 3). It revealed for the first time that the domain contains FAD and that it is structurally related to PHBH, the prototype of FAD-dependent aromatic monooxygenases ([65-68, 85] and references therein). In the light of its strong conservation, the mouse MICAL-1 MO can be taken as a valid model for the corresponding domain of all MICALs, although subtle differences may be the reason for some of the functional differences that will be discussed below. As for PHBH and related flavoenzymes, the core of MO is formed by a large domain (the FAD-binding domain, residues 1–226 and 373–484 with the mouse and human MICAL1-MO numbering) and a smaller one (residues 234–366) that we refer to as the cap domain for consistency with previous work [62, 86]. The connection between these domains is less complex than in PHBH involving β strands β9 (residues 227–233) and β15 (residues 367–373,), suggesting a greater conformational flexibility of MICAL-MO with respect to PHBH (Figure 3). MICAL MO lacks regions corresponding to the C-terminal dimerization portion of PHBH. Residues 1-71 [63] or 1-85 ([64], Figure 3) form a subdomain unique to MICAL, which precedes the core region. Here, several conserved basic residues (Lys-52, -61, -66, -69, and -86; Arg-35 and -70; His-11, -13, and -49) contribute, with other conserved residues of the FAD binding domain, to form a patch of basic electrostatic potential on one face of the protein (Figure 4A, circled). The latter has been proposed to be the docking site for an acidic protein partner, such as actin itself [64].

Another positively charged region is found on the opposite face of the MO domain (Figure 4B, white star). It most likely marks the NADPH binding site on the basis of the overall similarity between MO and PHBH and of the presence of several conserved basic residues that in PHBH contribute to NADPH binding [63, 64] (see also the sequence analyses in [62]). The FAD coenzyme binds to MO in an extended conformation as found in PHBH (Figure 5). At variance with the structures of PHBH in the oxidized forms ([65-68] and references therein), the “as isolated” MICAL-1 MO is in the “flavin out” rather than “flavin in” conformation (with the dimethylbenzene ring pointing towards the surface of the NADPH-binding region, Figures 3-5). The isoalloxazine ring of FAD (re-face) and Trp400 side chain are parallel and in close contact forming the charge-transfer complex that characterizes the MICALs spectra (Figure 2). The FAD/Trp charge-transfer complex is not shared with PHBH. Rather is reminiscent of enzymes of the ferredoxin:$NADP^+$ reductase family [87]. NADPH-treatment of mouse MO crystals led to a form in which one of the two subunits of the crystallographic dimer (chain A) contained reduced FAD [64]. In the other subunit a mixture of oxidized and reduced species was observed. Reduction caused a conformational change that shifted FAD from an “out” to an “in” conformation due to a rotation of the C3-C4 bond of the ribityl side chain. It was accompanied by a 6.5° rigid body rotation of the “cap” with respect to the FAD binding domain with the β9 and β15 connection acting as a hinge (Figures 3-5). The switch from the “flavin out” (oxidized) to the “flavin in” (reduced) conformation also increased to some extent the size of the cavity in front of the isoalloxazine ring, where the active site should be on the basis of the similarity with PHBH [64]. Furthermore, inspection of the protein face opposite to that with the proposed NADPH binding site revealed

the formation of a small channel that connects the surface to the active site, so that the FAD isoalloxazine ring seems now accessible (Figure 4 C,D). Interestingly, the mouth of such channel and the immediate surroundings of the flavin isoalloxazine ring involve highly conserved residues [62], among which is the 395 - 405 loop that contains Trp400 (Figure 3). These observations led Siebold et al. [64] to propose that a small molecule or, more attractively, a protein side chain could now access the MO active site from this side and be modified. The positive patch on the same side of the protein could help docking a hypothetical acidic protein substrate (e.g.: actin). Inspection of the region that should correspond to the MO active site revealed no evident similarity with PHBH or other well-characterized flavoenzymes. Thus, no further clues on the actual MO substrate and reaction mechanism were obtained [64].

The mouse MICAL-1 MOCH structure in the "as isolated" (oxidized) form was recently determined (Table 2, Figure 6, [76]). Note that the 4TTT code for the "native 2" structure appearing in Table 1 of [76], which we identify in Table 2 as structure 4TXK from the description and the Protein Data Bank, seems to correspond to the "Crystal structure of an O2-tolerant [NiFe]-hydrogenase from *Ralstonia eutropha* in its as-isolated form (oxidized state) – 3" (no accompanying publication). The structure of the MO domain is not altered in the presence of the CH domain [76]. At variance with previous analyses of the MICAL-1 MO structure [63, 64] and their direct inspection, the MO domain is now described as showing a "cavity that connects to the active site larger in MICAL-MO than in PHBH" so that it "could potentially accommodate a protein substrate" [76]. A "large opening" and a "small opening" that make the FAD coenzyme accessible from the surface [76] are now defined along with a "catalytic loop" in proximity of FAD isoalloxazine ring in the "in" conformation and being formed by conserved residues. If our reading is correct the "catalytic loop" is the 395 –405 loop containing Trp400 in MICAL-1 (Trp405 in MICAL-2, Figures 3, 6). Its conservation indicates that this loop is indeed important. For example, Trp400 should reposition to allow for hydride transfer from NADPH to the flavin during the catalytic cycle (see below). However, its precise involvement in catalysis remains to be established. The "large opening" should correspond to that on the MO face where the NADPH binding site is likely located. Here, the NADPH nicotinamide ring should reduce the flavin when in the "out" position by analogy with PHBH. The "small opening" mentioned in [76] should be the channel that connects the surface to the active site in the reduced protein form ([64], Figure 4). However, it cannot be ruled out that through even limited protein motions the MO active site may become accessible to small molecules. Overall, the cavity in proximity of the flavin isoalloxazine ring, where the active site should be located by analogy with PHBH, appears rather small in all structures available (see also Figure 4C, D of [64]).

The structure of the isolated MICAL CH domain was determined by NMR ([83] and several depositions in the PDB that are not accompanied by publications, Table 2). Sequence and structural comparisons led to the conclusion that it belongs to the Type 2 class. CH domains are found in several actin binding proteins where they serve to bind G- or F-actin [28, 88-92]. In spite of the conservation of motifs identified as actin binding sites, actin binding proteins typically contain two tandem CH domains. The C-terminal CH domains (defined as Type 2 or CH2 domain) do not bind G-actin and are not sufficient to bind F-actin. Rather, as

exemplified by α-actinin, it is the N-terminal Type 1 CH domain (or CH1 domain) that is mainly responsible of binding to the filament [88-92]. Accordingly, [83] did not observe CH binding to G- or F-actin.

The high resolution structure of mouse MICAL-1 MOCH ([76], Table 2, Figures 6 and 7) confirmed the assignment of the CH domain to the Type 2 class and confirming the high similarity with α-actinin (PDB 2EYI, [93], 4D1E [94]) CH2 domain, taken as a well-characterized example of actin binding proteins containing tandem CH domains. The 19 residues connecting the MO and CH domains were not visible in the crystal structure and multiple options were found for the structure of the MOCH protein [76]. Association of the MO and CH domain of the same polypeptide chain was done thanks to small-angle X-ray scattering experiments (SAXS) in solution leading to the model in Figure 6. A similar model was obtained by us with the human MICAL-1 MOCH by SAXS (unpublished). The MOCH structure shows no contacts between the domains in agreement with the similar spectroscopic and kinetic properties of the human MICAL-1 MO and MOCH forms [78, 79]. The residues corresponding to the actin binding site and a potential phosphatidylinositol bisphosphate (PIP2) binding site are shown in Figures 6 and 7. Interestingly, to our knowledge the interaction between MICAL and PIP2, which could function as a biologically relevant regulator [95], has not been studied yet.

The role of the CH domain in MOCH has been explored through a series of kinetic studies that will be discussed below [76, 79]. Interestingly, the mouse MICAL-1 MOCH structure was used for *in silico* docking experiments to generate a model of the MOCH/F-actin complex [76], which will be discussed later in conjunction with the presentation of the reaction of MICAL in the presence of actin filaments.

The structure of human MICAL-1 LIM domain has also been determined by NMR (Table 2, Figure 7). This domain is formed by two tandem zinc fingers and is found in a broad family of proteins that participate in cytoskeleton organization, signal transduction, cell adhesion, gene expression regulation [28, 96-99]. Little is known about its precise function in MICAL and MICAL-like proteins. From experiments in which various forms of MICAL were expressed in cell lines it may be important for the interaction with some MICAL protein partners such as, e.g.: CRMP proteins [41]. As an alternative, it may have a role in organizing the other MICAL domains. Whether it is fully responsible of the partial dimerization we observed in full-length MICAL (see above) or it participates in the so-called autoinhibition of MICAL exerted by the MICAL's C-terminal region [41] still needs to be established.

In this respect, the initial observation that MICAL is recruited and activated by binding to semaphorin-activated PlexA through its C-terminal region led to the hypothesis that this part of the protein plays an important role in stabilizing an inactive conformation of MICAL in the free state. Inhibition would be relieved when this region is engaged in interactions with other protein (the cytoplasmic side of PlexA, CasL , proteins of the Rab family or even NDR1/2). This hypothesis was strongly supported by the experiments of Schmidt et al. [41] with studies in selected cell lines and cell extracts and, later, was confirmed with purified proteins [32, 79]

The C-terminal region of MICAL-1 and -3 are conserved within each protein class. They share, as common features, the Pro-rich and Glu-rich regions mentioned above and motifs for the formation of CC. As mentioned before, MICAL-2 is organized differently with the protein ending after the LIM domain. However, a Pro-rich region and a motif consistent with the potential formation of helical structures was identified in the region between the CH and LIM domains, and the short segment after the protein C-terminus may also form a helical structure (Figure 1, [62]).

Our understanding of this part of MICAL has made progress since the recent publication of the structures of its C-terminal region where consensus sequences for CC formation were found [32, 69].

The C-terminal part of human MICAL-1 (residues 918-1067 [32, 69]) and the corresponding regions of human MICAL-3 (residues 1841-1990, [69]) were produced along with several variants [32, 69]. The corresponding fragments of human MICAL-cL (a MICAL-like protein containing only the C-terminal region) and of EHBP-1 and -2 (from Eps15-homology domain binding proteins-1 and -2), which were identified by sequence analyses were produced and analyzed as well [69].

These proteins were found to be sufficient for binding several proteins of the Rab1 (Rab1a, Rab1b and the related Rab35) and Rab8 (Rab8, Rab10, Rab13 and Rab15) family of small GTPases. But the stoichiometries and binding affinities differed (see below). Thus, the domain will be called RBD for Rab binding domain to facilitate the presentation.

The structure of the human MICAL-1 RBD was solved in complex with two copies of Rab10 ([69], Table 2) and in the isolated form ([32], Table 2). The MICAL-1 RBD *per se* is monomeric and forms three α-helices arranged to yield a compact curved surface ([32, 69], Figure 8). Only a few fragments in the N- and C-terminal part as well as in the loops connecting the helices are disordered. The complex between MICAL-1 RBD and Rab10 (a member of the Rab8 family) showed the two Rab binding sites inferred from binding studies in solution with Rab8A that led to identify a high affinity site (K_d ~50 nM) in the first part of the RBD and a lower affinity site (K_d in the low μM range) in the second part. Accordingly, one Rab10 molecule mainly binds to residues of helix 1 and helix 2 (in part) in the first half of MICAL RBD and the second to helix 3 and helix 2 (in part) at the C-terminus (Figure 8).

The RBD of MICAL-3 ([69], Figure 8) forms dimers with each subunit being similar to the MICAL-1 RBD monomer [69]. The two copies of MICAL-3 form a central 4-stranded coiled-coil composed of α-helices 2 and 3 of each monomer flanked by α-helices 1 on both sides. Interestingly, such intersubunit interactions overlap with the second (C-terminal, low affinity) binding site of MICAL-1 RBD, which is also observed in MICAL-cL in complex with several Rab proteins ([69], Table 2). This finding explains why the RBD of MICAL-3 migrates in gel filtration as a dimer, but incubation with Rab8 seems to generate a complex involving one molecule of MICAL-3 RBD and 2 molecules of Rab8. Furthermore, there is an excellent match between the residues that appear to be essential for Rab35 binding [32] and those in the second Rab binding site of the Rab10/MICAL-1 complex of Rai et al. [69].

Consistent with the presence of two Rab binding sites in the RBD of MICAL-1 and MICAL-3 is the formation of a ternary Rab8:MICAL-1:Rab6 complex, which was detected in cells [33].

Further work is needed to fully explain the molecular reasons of the different specificity of the Rab binding sites. However, it has been established that the N-terminus of Rab seems important, as well as the presence of GTP that stabilizes the active conformation of Rab. On the contrary, the prenylation state of Rab does not seem to influence its interaction with MICAL's RBD [32, 69]. The structural work also revealed that the two halves of the RBD of human MICAL-1, MICAL-3, MICAL-L1, MICAL-L2, MICALcL and also EHBP1, EHBP1L1 and C16orf45 (encoding an unknown protein) seem to be derived from each other through gene duplication, thus generating the family of bivalent MICAL/EHBP Rab binding (bMERB) domains as defined in [69] (Figure 9).

An attempt to gain information on the region between the LIM and RBD of human MICAL-1 was done in preparation of this review using the Robetta web server (http://robetta.bakerlab.org/, [100]). Robetta correctly identified and modelled all MO, CH. LIM and Rab binding domains for which structural information is available. Region 779 – 907 was detected as an independent domain and it was modelled using the structure of a DNA polymerase III, γ subunit-related protein (tm0771) from *Thermotoga maritima msb8* at 2.00 Å resolution (PDB ID: 2GNO) as template suggesting that it is an α/β globular subdomain. However, the sequence similarity with DNA polymerase γ subunit, which is important as it forms the sliding clamp of DNA polymerase and, interestingly, has ATPase activity, is very low.

The high resolution structure of full-length MICAL has not been presented yet. However, with methods for its production and purification available it is likely work in that direction is in progress in several laboratories. Information on the structure of human MICAL-1 forms is being acquired also in our laboratory by solution studies by small-angle X-ray scattering in collaboration with the Svergun's group [101-103].

Catalytic and mechanistic properties of MICAL forms.

Nadella et al. [63] were the first ones to show that mouse MICAL-1 MO exhibits a strong NADPH-dependent H_2O_2-producing NADPH oxidase activity (Figure 1B). Later, the Terman group demonstrated the NADPH-dependent F-actin depolymerizing activity that makes MICALs unique among actin binding proteins [70]. These seminal findings were followed by a variety of studies with different approaches by different groups with results that have led to sometimes significantly different conclusions. The biological effects of the NADPH oxidase activity of the free enzyme, which produces a reactive oxygen species (ROS), need to be precisely established. Whether the enzyme switches from a NADPH oxidase (in the free state) to a hydroxylase (when F-actin bound) that modifies specific actin residues or the actin depolymerizing activity is mediated by H_2O_2 produced by the NADPH oxidase reaction is a matter of debate. While there is general agreement on the fact that the C-terminal region of MICAL-1 and -3 is crucial for the switch from an "autoinhibited" to an active MICAL form, the precise properties of the "autoinhibited" form require further

investigation. The role of the other domains in promoting MICAL autoinhibition or activation still needs to be elucidated. Furthermore, it is not clear if all proteins that bind to the C-terminal region of MICAL (CasL, the cytoplasmic side of semaphorin-activated plexin, Rab, and even NDR that make MICAL function as an anti-apoptotic factor) stabilize the active form of MICAL. The CH domain was postulated to promote MICAL/F-actin interaction based on the fact that several F-actin binding proteins contain CH domains. Whether the hypothesis is supported by experimental evidence will be discussed. Whether MICAL's reaction causes F-actin severing or dissociation of actin monomers from the filament ends is also under discussion. It still remains to be determined where other MICAL interactors (e.g.: CRMP) precisely bind, and if they may be also substrates or activators of MICAL. A precise understanding of MICAL's mechanistic properties would also help the search of inhibitors as leads for novel drugs. Also this issue requires further work.

In this section an attempt will be made to summarize the experimental evidence available on mechanistic aspects of MICAL and the various theories. Efforts to reconcile some discrepancies in the literature will also be made with the aim to contribute to the understanding of how these complex enzymes may actually work *in vitro* and *in vivo*.

The NADPH oxidase activity of MICAL.

Nadella et al. [63] demonstrated that mouse MICAL-1 MO catalyzes a NADPH oxidase activity by assaying H_2O_2 production in a coupled assay with horseradish peroxidase (HRP) and Amplex Red. The reported apparent k_{cat} and K_m for NADPH ($K_{m,NADPH}$) value were 77 s^{-1} and 222 μM, respectively, calculated by varying NADPH concentration at fixed (atmospheric) oxygen concentration at 25°C in 20 mM Hepes buffer, pH 7.0, containing 100 mM NaCl. Human MICAL-1 MO was confirmed to catalyze a NADPH oxidase reaction with apparent k_{cat} of ~ 3 s^{-1} and $K_{m,\ NADPH}$ of ~ 20 μM in the same buffer, but in the absence of NaCl (Table 3, [78]). The differences in $K_{m,NADPH}$ could be readily justified by taking into account the high sensitivity of human MICAL-1 MO to the ionic strength of the assay medium and also to the type of anions present [78]. With human MO (and the other MICAL forms), increasing ionic strength has a moderate effect on k_{cat}, but leads to significant drop of $k_{cat}/K_{m,NADPH}$ due to an increase of $K_{m,\ NADPH}$, a property that actually reinforces the similarity with PHBH [104]. The almost 20-fold difference in k_{cat} between the mouse and human properties may be rationalized by taking into account artifacts arising from the coupled assay with HRP and Amplex red [78] and by reanalyzing the raw data reported in Figure 5 of Nadella et al. [63]. NADPH was found both to inhibit the HRP reaction and to lower the total amount of H_2O_2 that could be quantified [78]. On the other hand, the rate of NADPH oxidation (as measured by absorbance changes at 340 nm) was increased by HRP, Amplex Red (or o-dianisidine) and H_2O_2 ([78], and unpublished observations). Figure 5 of [63] shows spectra recorded at different times during an assay done in the presence of 0.1 mM NADPH and 6 nM mouse MICAL-1 MO, HRP and Amplex Red. If our calculations are correct, analysis of the raw data leads to an initial velocity (expressed as v/E) of ~13 s^{-1} (from the absorbance changes at 340 nm) and of ~ 5 s^{-1}(from the absorbance changes at 560 nm and 570 nm due to Amplex Red oxidation). The latter v/E value is close to that measured with human MICAL-1 MO (~ 3 s^{-1}, Table 3). The origin of the

initial velocity value of approximately 0.11 μM NADPH oxidized per second shown in the inset of the figure at 100 μM NADPH [63] is not clear. It would translate in a v/E of 18 s^{-1} at 6 nM enzyme. Interestingly, 0.11 roughly corresponds to the change of absorbance of Amplex Red during the first minute of reaction shown in the figure. The same laboratory now reports a kcat of 0.68 s^{-1} and a $K_{m,NADPH}$ of 28.8 μM for the same mouse MICAL-1 MO [76]. These values, which were obtained by directly monitoring NADPH oxidation at 340 nm (in the absence of reaction components other than buffer, NADPH and oxygen), are also unexpected. The quoted $K_{m,NADPH}$ is much lower than that expected by taking into account the fact that these assays were carried out in the high ionic strength buffer used to stabilize F-actin (F-buffer, 5 mM Tris/HCl, pH 8.0, containing 50 mM KCl, 2 mM $MgCl_2$, 1 mM ATP and 1 mM DTT). For comparison a $K_{m,NADPH}$ in the range of 500 μM was measured with human MICAL-1 MO in a similar buffer due to a combination of ionic strength and pH effects (Table 3, [78, 79]). The reported k_{cat} value of mouse MO (0.68 s^{-1}) is also approximately 5-6 fold lower than the corresponding value obtained with human MICAL-1 MO (~3 s^{-1}). An attempt to rationalize these discrepancies will be done in the next section in conjunction with the description of MICAL activity in the presence of F-actin.

The NADPH oxidase activities of full length human MICAL-1 protein of truncated forms progressively lacking the C-terminal region and the LIM domain (indicated as MICAL, MOCHLIM and MOCH, respectively) was studied in comparison with that catalyzed by the corresponding isolated MICAL-1 MO [78, 79]. As summarized in Table 3, the CH, LIM and C-terminal domains lead to a progressive increase of the apparent $K_{m,NADPH}$, which seems to reflect the changes of the overall protein charge as the acidic CH (pI, 4.6), LIM (pI, 5.3) and C-terminal regions (pI, 5.2) are added to the basic MO domain (pI, 9.1) in agreement with the know importance of electrostatics for NADPH binding to enzymes of the PHBH family. The apparent k_{cat} values of the MO, MOCH and MOCHLIM forms are similar to each other. On the contrary, the k_{cat} of the full-length protein is only ~10% that of the other forms confirming that the C-terminal domain inhibits the catalytic activity of the MO domain [41], but with purified protein [79]. All MICAL forms are very sensitive to the ionic strength of the medium and the identity of anions present, which mainly cause an increase of $K_{m,NADPH}$. This property reinforces the similarity between MICAL-MO and PHBH, but also complicates kinetic analyses. For example, the pH profiles of the apparent steady-state kinetic parameters of the NADPH oxidase reaction had to be determined in a mixed buffer that minimized the effect of different anions and maintained the ionic strength low and constant throughout the explored pH interval [78, 79] (Figure 10). All curves were complex. $k_{cat}/K_{m,NADPH}$ and $1/K_{m,NADPH}$ values decreased from high values as the pH increased in a biphasic fashion. The shape of the curves most likely reflected the overall charge of the protein forms as a function of pH, rather than the effect of the protonation state of specific groups on the parameters [79]. In particular, the pH profile of $1/K_{m,NADPH}$ is reminiscent of the $1/K_{d,NADPH}$ profile determined in PHBH [104] further reinforcing the similarity between MICAL MO and PHBH. The k_{cat} profiles of MO and MOCH were similar to each other. k_{cat} increased from a low non-zero value at low pH to a maximum at about pH 8 and then decreased to another non-zero value at high pH, perhaps indicating a change of the rate determining step of the reaction, which still needs to be explored. Fitting of the curve

suggested the presence of a group with pK_a of 6-6.5 that needs to be deprotonated and of another with a pK_a of 8.5 -9 that needs to be protonated to reach maximum values of k_{cat}. Inspection of mouse MICAL-1 MO structures did not allow to identify any candidate for the observed pK_a values, which are similar to those found in the $k_{cat}/K_{m,NADPH}$ and $1/K_{m,NADPH}$ profiles (Figure 10). Among residues in proximity of FAD, which marks the active site, only His126 may exhibit a pK_a of 6-6.5. This residue is conserved in all MICAL MO and may stabilize the "flavin in" conformation through hydrogen bonds between its main chain atoms and the isoalloxazine N(3) and O(4) atoms (Figure 5). The local charge may influence the interaction. Arg121 and Asp393 interact with the ribityl side chain (Figure 5). They may also contribute to the stabilization of the flavin in or flavin out conformation, and, therefore, influence the turnover rate. However, their pK_a values cannot be readily identified with those that allowed to fit the pH profile of k_{cat} with MO and MOCH. Spectra of human MICAL-1 MO and MOCH samples diluted in buffers at pH between 5 and 9-10 did not show any change except for evident signs of protein denaturation at pH above 8.5 – 9 ruling out that the protein overall charge or that of selected residues affects the stability of the FAD/Trp400 charge-transfer complex [79]. With MOCHLIM, k_{cat} values increased from low values at pH 5, which were similar to those observed with MO and MOCH at the same pH, to a constant value at pH 6 to 9, similar to the maximum k_{cat} value obtained with MO and MOCH. The k_{cat} of full-length MICAL decreased from a high value at pH 5 to constant values in the explored pH range, which was limited by a combination of low activity, high $K_{m,NADPH}$ and protein stability. For this protein form the increase of k_{cat} at low pH may reflect the loosening of the interactions between the MO domain (pI, 9.1) and the C-terminal region (pI, 5.2) due to the decrease of negative charge of the C-terminal region. However, the k_{cat} value remained low indicating that if the increase of k_{cat} at low pH is related to the titration of acidic regions of the protein, its isoelectric point should be well below 5. The Glu-rich portion of the C-terminal domain preceding the RBD of MICAL-1 may have a pI as low as 3.7 (calculated for the 858-900 region of MICAL-1).

The rate of reduction by NADPH of human MICAL-1 MO was also studied directly by rapid reaction kinetics under anaerobiosis in 20 mM Hepes/NaOH buffer, pH 7.0, 10% glycerol [78]. No reaction intermediates could be detected by comparing absorption changes at different wavelength. Complete FAD reduction took place in a single phase at a limiting rate of ~3 s^{-1} with a K_d for NADPH of 56 μM. Both values matched well the steady-state k_{cat} and $K_{m,NADPH}$ values once the presence of 10% glycerol in the stopped-flow experiment was taken into account. Thus, the rate of enzyme reduction by NADPH, which in the stopped-flow experiment is independent from protein concentration determination, and may also detect the presence of enzyme forms exhibiting different activities, appears to fully limit turnover.

The study of solvent viscosity effects both highlighted the presence of a rate determining conformational change in the enzyme reductive half reaction and helped to clarify the possible origin of the low k_{cat} of full-length MICAL [79]. The solvent viscosity effect on $k_{cat}/K_{m,NADPH}$ was greater than one for all MICAL forms detecting a conformational change between NADPH binding and either flavin reduction by NADPH or $NADP^+$ release from the reduced enzyme whose rate is relatively slow and contributes to the value of this parameter. The decrease from ~ 2.7 (MO), ~2.3 (MOCH), ~1.8 (MOCHLIM) and ~1.7 (MICAL) correlates

well with the increase of $K_{m,NADPH}$ that partially "suppresses" the effect. Indeed, for a large K_m value the parameter would be determined by diffusion of NADPH towards the enzyme active site and the value would be 1. By analogy with PHBH, several conformational changes may take place during the MICAL MO catalytic cycle [65, 67, 68]. In a minimal scheme for MICAL, one conformational change could take place prior to flavin reduction, i.e.: Trp400 must probably move away from the position observed in oxidized MO to allow the correct positioning of NADPH nicotinamide ring for hydride transfer (Figure 5). Upon reduction the switch from the flavin out to the flavin in conformation must take place. $NADP^+$ is a competitive inhibitor with respect to NADPH with a K_i of 77 μM [78] and titrations of MICAL-MO with NADPH indicate that the reaction equilibrium lies towards products with a K_{eq} of approximately 0.59×10^6 for the overall equilibrium between oxidized MO and NADPH and reduced MO and $NADP^+$ [78]. For all these reasons the working hypothesis is that the solvent viscosity effect on $k_{cat}/K_{m,NADPH}$ detects the repositioning of Trp400 in order to allow the NADPH nicotinamide ring to approach flavin N(5) position. In the light of the match between k_{red} in the stopped-flow and k_{cat}, and the absence of detectable intermediates, the solvent viscosity effect of 1 on k_{cat} likely indicates that a high solvent viscosity effect due to the relatively low rate of the conformational change preceding hydride transfer is offset by the fact that also hydride transfer is rate determining. The similar values of the solvent viscosity effects on k_{cat} and $k_{cat}/K_{m,NADPH}$ for the four MICAL1 forms indicate that the relative magnitude of the steps of the reaction catalyzed by the MO domain is unchanged in the presence of the CH, LIM and C-terminal regions. Thus, with the information that k_{cat} for MO, MOCH and MOCHLIM are very similar, it could be concluded that the low k_{cat} value of full length MICAL is likely due to the fact that it reflects the presence of a fraction (~10%) of enzyme in a fully active conformation in equilibrium with a fully inactive form (~90%). If the high K_m for NADPH reflected the overall charge of the protein, one would expect that full length MICAL in the active conformation exhibited a $K_{m,\ NADPH}$ as high as that of MOCHLIM, thus in the 0.3 – 0.5 mM range, but a k_{cat} of approximately 3 s^{-1}. Rapid reaction studies of the isolated half reactions of the various MICAL forms could be very informative. These studies have been limited so far by their tendency to aggregate at low ionic strength at the high concentration required for stropped-flow work. The need to include salt to avoid aggregation leads to high K_m (K_d) values for NADPH so that complete analyses become difficult.

A rapid reaction (stopped-flow) approach was mainly used to study mouse MICAL-2 MO [77]. The rate constant for enzyme reduction by NADPH, which occurred without detectable intermediates, was 0.07 s^{-1} and the K_d for NADPH was 0.5 – 0.9 mM with the enzyme in 20 mM Hepes buffer, pH 8.0 and 4 °C. These results indicated that mouse MICAL-2 catalyzes NADPH oxidation at a much lower rate than the corresponding MICAL-1 form, a fact that has been qualitatively confirmed later [46].The K_d for NADPH was also high. The studies of mouse MICAL-2 MO also determined that the enzyme, like PHBH, transfers the 4-proR hydrogen from NADPH to the flavin; the kinetic deuterium isotope effect on the isolated reductive half reaction was 4 ruling out that a conformational change rather than hydride transfer could contribute to k_{red}. A mid-point potential of the FAD_{ox}/FAD_{red} couple of -240 mV was determined in 20 mM Hepes buffer, pH 8.0. It is more negative than the estimate of the corresponding value of ~ - 0.15 V for

human MICAL-1 MO at pH 7 [78]. The different mid-point potentials of the bound FAD may even explain the approximately 50-fold difference in reduction rate between MICAL-1 and MICAL-2 MO domains.

The recent publication of methods to produce drosophila MICAL MOCH was not accompanied by a kinetic characterization of the catalyzed reaction [74]. From the data presented in Figure 3C of the same paper, the NADPH oxidase reaction appears slow (v/E, 0.018 s^{-1} at 100 μM NADPH, pH 8.0, with 600 nM enzyme).

From a biological point of view, the NADPH oxidase activity of full-length MICAL may be sufficiently high to generate H_2O_2 that may act as a second messenger and could modulate the activity of other proteins through oxidation reactions, especially if the MICAL's activating proteins determine where and when H_2O_2 is produced. Furthermore, the high $K_{m,NADPH}$ suggests that the local concentration of NADPH determines the rate of H_2O_2 production assigning another potential regulatory role to this compound [105, 106]. The importance of redox regulation for cytoskeleton proteins and their organizers is known (see, e.g., [107-109]). Increased levels of ROS have been directly correlated with those of MICAL-1 and -2 in normal and cancer cells [41, 54, 55, 59]. Furthermore, it has been proposed that MICAL's H_2O_2-producing NADPH oxidase reaction regulates the biological activity of CRMP2 [42, 107, 110], a member of the CRMP family of important regulators of the cytoskeleton and also mediators of semaphorin signaling, which interact with plexin receptors ([21, 41]; see below). Whether and how the NADPH oxidase activity of MICAL-MO is implicated in the F-actin depolymerizing reaction that makes MICAL unique among regulators of cytoskeleton dynamics is discussed in the next section.

MICAL and F-actin.

Since the discovery that MICAL participates in the transduction of the signal initiated by semaphorin binding to their plexin receptors, which results in local actin cytoskeleton disassembly, the hypothesis that it functioned as an actin-binding protein destabilizing the actin filament was made. The essentiality of the integrity of the N-terminal flavoprotein domain for the function was also inferred from the "loss-of-function" phenotype obtained by expressing variants in which all the three glycine residues of the GXGXXG motif in the Rossman fold for FAD binding were substituted by Trp residues. This rather drastic mutation is commonly used in *ex-vivo* and *in vivo* studies to establish the involvement of MICAL's catalytic activity in a given function. The finding that the flavoprotein domain is structurally similar to PHBH [63, 64] and that it catalyzes a NADPH-dependent F-actin depolymerization [70] soon led to the hypothesis that MICAL disassembles F-actin by oxidizing an actin side chain and, eventually, that MICAL MO domain, as a member of the PHBH family, switches from an H_2O_2-producing oxidase activity, in the free state, to the specific hydroxylation reaction of its "authentic substrate" (Figure 1B). The bound authentic substrate would both control the reaction mechanism and enhance the enzyme catalytic efficiency. Mass spectrometry analysis of mammalian and drosophila actin that had been re-purified by ion exchange chromatography after incubation with drosophila MICAL MOCH showed that actin molecules had been oxidized by incorporating two oxygen atoms [71]. Among actin residues, only Met44 and Met47 were found to be oxidized to presumably

yield methionine sulfoxide. Testing of the behavior of MOCH with actin Met44L and Met47L variants showed that intactness of Met44 was crucial in order to observe NADPH-dependent MICAL-mediated actin disassembly [71]. The Met residues belong to actin D-loop at the interface between monomers in the filament (see, e.g.: [111]). These residues are at a critical position in the filament and are also particularly sensitive to oxidation [112]. It was later shown that R specific methionine sulfoxide reductases (mammalian MsrB, [75] and the drosophila homolog SelR [72]), but not the enzymes specific for the S isomer, reversed the modification of both actin Met residues demonstrating that Met44 and Met47 had been converted to methionine sulfoxide and indicating that only the R stereoisomer of methionine sulfoxide was generated at actin positions 44 and 47 by the MICAL reaction. Thus, the released modified actin monomers could be repaired, *in vivo*, by R-specific methionine sulfoxide reductases [113]. By direct observation of actin filaments that had been treated with MICAL, it was also concluded that MICAL severes them leading to actin fragments, which would then disassemble releasing monomers [71, 73]. Very recently, the modification of Met44 and Met47 (the latter residues being sometimes neglected in the discussion of mechanistic models of MICAL reaction with actin) was confirmed by observing protection of actin from subtilisin cleavage and using antibodies specific for the methionine sulfoxide derivative of actin [73]. The drosophila MICAL-modified actin monomers were found to be actually still able to polymerize, but with slower kinetics and higher critical concentration for the initial nucleation events as compared to native actin [73]. By studying the NADPH-dependent actin depolymerizing activity of drosophila MICAL-MOCH in the presence of cofilin it was also proposed that Met44 (and Met47) oxidation of actin catalyzed by MICAL makes the filament more susceptible to the severing activity of cofilin so that – *in vivo* - MICAL and cofilin can cooperate in F-actin disassembly. From the resistance of actin to subtilisin digestion it was also concluded that full modification of actin Met by drosophila MOCH took place during the first minute of incubation, while disassembly was significantly slower in the absence of cofilin. In these interesting experiments the MICAL MOCH reaction was apparently quenched at different incubation times by adding $NADP^+$ and kabiramide C (to sequester actin monomers). Whether $NADP^+$ addition (1.5 mM) is sufficient to block the NADPH-dependent MOCH reaction has not been shown. For human MICAL-1 MO $NADP^+$ acted as competitive inhibitor with respect to NADPH, but the K_i was high (1.7 mM) in the presence of 0.1 M NaCl. Other methods may be more efficient to block the reaction like the glutamate synthase-catalyzed conversion of NADPH into $NADP^+$ used in [78]. However, that filament disassembly is slower than chemical modification by MICAL was independently confirmed by monitoring single actin filaments in a microfluidic set-up [32]. Fremont et al. [32] directly observed that human MICAL-1 forms cause the NADPH-dependent depolymerization of actin filaments by accelerating the release of monomers from their ends. Thus, a severing activity of MICAL could not be confirmed not even reproducing the experimental set up described by [71, 73]. The rate of monomer release with MICAL MOCH (600 nM) from the filaments increased during the first 2 minutes of treatment and reached a plateau value of 50 actin monomers released per second, a value 5-10- fold higher than that measured in the absence of MICAL, or NADPH. Interestingly, enhanced depolymerization was observed also after MICAL MO and NADPH were washed away from the capillary,

demonstrating that MICAL-oxidized actin filaments depolymerize faster regardless of the presence of the enzyme

For the modification of actin Met44 and Met47 through a specific hydroxylase activity of the MICAL MO domain, the D-loop of actin, which is at the interface between monomers in the filament, should be "extracted", enter the MO active site where the residue(s) would be stereospecifically hydroxylated and then converted to the R isomer of the methionine sulfoxide derivative. Eventually, the modified D-loop would be released to yield a destabilized filament that would disassemble spontaneously or, more rapidly, with the assistance of cofilin. A cooperative effect between MICAL and cofilin has been proposed previously [107]. However, in that case, MICAL was proposed to control cofilin by oxidizing it through the H_2O_2 released by its NADPH oxidase activity. Interestingly, cofilin did not prevent the interaction of drosophila MICAL MOCH with F-actin when the three proteins were present at similar concentrations, placing restraints on how MICAL MO may bind to F-actin.

An interesting attempt to model the F-actin-bound MICAL was done using the crystallographic structure of mouse MICAL-1 MOCH [76]. In the simulation the MICAL CH domain was reportedly docked on an F-actin dimer (PDB ID: 2ZWH, [114]) by mimicking the binding mode of α-actinin CH1 domain to F-actin as derived by (cryo)EM experiments (3LUE, [92]). Furthermore, the hypothesis was made that MICAL MO directly hydroxylates actin Met44 and converts it into methionine sulfoxide (see below for further discussion of this reaction). Thus, the simulations were performed by positioning the MO with the "large opening" towards the actin filament model. Then, a series of simulations was performed in which Met44 sulfur was constrained to get closer to the flavin C4a position until it reached a distance of approximately 3 Å [76]. In the resulting model it appears that MICAL MO interacts with F-actin close to the interface between monomers with the face where the proposed NADPH binding site is (Figure 11). The D loop of one actin monomer has been extracted from its original position and Met44 sulfur is in front of flavin N5 position. The Met44 sulfur seems to occupy the position of Trp400 CZ3 carbon atom, which must have been displaced along with the 395-405 loop (Figure 11, bottom panels). The authors [76] conclude that hydroxyl transfer from the 4a-hydroperoxide intermediate, which would be formed upon reaction of the reduced flavin with oxygen, could take place even when the flavin is in the "in" position.

This model is very attractive, but it would rule out the equally attractive hypothesis of Siebold et al. [64] that NADPH and the (actin) substrate can bind in a non-mutually exclusive way to opposite faces of MO. Further work is certainly needed to fully reconcile the models above with the entire body of evidence available on the catalytic activities of MICAL forms, which is illustrated below.

The rate of NADPH oxidation catalyzed by all MICAL forms tested increases significantly in the presence of F-actin but not in that of G-actin, as shown for the first time with human MICAL-1 MO ([62, 78, 79], Figure 12). This is the behavior expected for a monooxygenase related to PHBH in the presence of its substrate undergoing hydroxylation. However, for a stereospecific hydroxylation reaction leading to formation of the R isomer of a methionyl-sulfoxide side chain, one would expect stereospecific modification

of one methionine residue (Met44) rather than two (Met 44 and Met 47) with equal efficiency. In any case, if Met44 and Met47 on actin D-loop were the substrates of a specific hydroxylase activity, one would expect a biphasic time-course of NADPH consumption. In a first phase NADPH should be rapidly oxidized in an amount corresponding to twice the total actin monomer concentration. Then, a second slow phase of NADPH oxidation would follow due to the NADPH oxidase activity observed in the absence of actin (Figure 12). Instead, as initially shown for human MICAL-1 forms [78, 79] and later confirmed with other MICAL species [73, 76], fast consumption of all NADPH present is observed even when NADPH exceeds by far total actin monomers concentration. In some assays, the initial part of the curves describing the time-course of NADPH oxidation seemed to suggest the presence of a small initial faster rate [76, 78]. However, at least for human MICAL-1 forms, an initial fast phase is not always evident. Furthermore, it does not correlate with the initial F-actin concentration as expected for a "burst phase" in which the rapid and specific methionine hydroxylase activity would be followed by a slower NADPH oxidase reaction. On the other hand, at variance with the report of biphasic traces in the presence of actin [76], the traces shown for the reaction of mouse MICAL-1 MO and MOCH with NADPH (100 μM) and different F-actin concentrations show some biphasicity only with MOCH when F-actin is absent (see Supplementary Figure S4 of [76]). The difficulty to work with a viscous substrate like F-actin, in small reaction volumes (100 – 200 μl) due to the actin cost, is probably the reason for anomalies of the traces at the early reaction times one sometimes observes.

The time-course and extent of NADPH consumption (Figure 12) could be interpreted in several ways [62, 78, 79] and the recent data can help clarify the situation [32, 73]. In all cases, F-actin activates MICAL's NADPH oxidoreductase activity (Figure 12, Table 3). MICAL MO properties predict that conformational changes take place as it cycles through the oxidized "flavin out" and reduced "flavin in" conformation. These conformational changes could be sufficient to mechanically destabilize the actin filament. The released monomers could repolymerize allowing for a steady-state level of filaments that would allow for multiple turnovers in a NADPH oxidase activity stimulated by F-actin. Thus, the MICAL-catalyzed actin depolymerization would be reversible, leading to the observed case of "substrate recycling" ([78], Figure 12). According to such mechanical effect of MICAL, actin modification would be accidental making the hypothesis unlikely. As an alternative, the actin monomers dissociate from the filament because of oxidation through *in situ* release of H_2O_2 by the NADPH oxidase activity. If actin chemical modification were significantly faster than actin disassembly, the filament could last enough to activate MICAL reaction with NADPH for multiple catalytic cycles. The apparent case of "substrate recycling" would be operative also in this case. The same would hold if – beside the slow filament disassembly – one took into account the fact that oxidized actin monomers can reassemble, as recently shown [73]. In all these cases MICAL should function as a NADPH oxidase with F-actin playing a stimulatory role. According to another hypothesis, MICAL bound to actin could function as a hydroxylase (specifically converting Met44 and Met47 into the methionine sulfoxide derivatives at early reaction times) but also as a NADPH oxidase releasing H_2O_2 directly on the filament (at a fast rate due to the activating effect of F-actin also on this activity).

To test this hypothesis the modification of actin that had been incubated with the human MICAL-1 forms and NADPH was analyzed by MALDI-TOF and mass spectrometry [79]. For these experiments the entire MICAL-treated actin population was analyzed by precipitating aliquots of the reaction mixture at different times (corresponding to different amounts of NADPH being oxidized). The analysis of MICAL-treated actin after the extensive manipulation described by [71] (buffer exchange by repeated dilution/concentration in centrifugal concentrators, followed by ion exchange chromatography and further concentration/dilution cycles for buffer exchange of the purest actin fractions) could have led to loss of unstable actin species and specific enrichment of others. Catalase was also included to scavenge any H_2O_2 released in solution although DTT is present in the F-actin stabilizing buffer used for the experiments [79]. Finally, actual catalytic amounts of MICAL forms were employed in order to complete the reaction in 20-60 min (e.g.: MOCH 10-30 nM with ~ 20 µM prepolymerized actin) as opposed to the higher drosophila MICAL MOCH concentrations (600 nM with 1.1 µM actin for 90 min).

Analysis of actin samples withdrawn at the early reaction stages had modification levels below detection, making unlikely a fast hydroxylation reaction of Met44 and Met47 followed by non-specific modification of other residues through *in situ* production of H_2O_2 by the NADPH oxidase activity. With samples withdrawn at longer incubation times, MALDI-TOF analyses of human MICAL-1-treated actin were consistent with oxidation of two-three residues in each actin molecule. Analysis of peptides obtained after proteolytic fragmentation of MICAL-treated actin showed modification of Met44 and Met47, but that also other residues had been modified with equal probability. The modified residues (Met 44 and Met47 on the actin 19-50 and 40-50 fragments; Met269 or Met 283 on actin 255-282 peptide; Met355 or Trp340 or Trp356 on actin 329-359 fragment and Met82 or Trp79 or Trp86 on the 69-99 peptide) are located near the interface between actin monomers in the filament (Figure 13). Among them Met269 and Met355 are closer to Met44 and Met47 than the other residues.

These results are in contrast with those obtained with the drosophila [71] and mouse MICAL forms [75] with which only actin Met44 and Met47 were found to be oxidized. While it is difficult to explain the discrepancy, which may reside in the different experimental setup, the findings with the human protein are consistent with the fact that when MICAL MO binds to F-actin, most likely at the interface between subunits, the NADPH oxidase activity of the MO domain is stimulated leading to enhanced *in situ* production of H_2O_2 that would be able to modify several actin residues [79]. The geometry of the complex could even cause (stereo)specificity of chemical modification of actin residues. Release of MICAL from the filament with return to the basal NADPH oxidase activity would limit the number and type of modified residues. Furthermore, with a H_2O_2-mediated actin modification, a 1:1 stoichiometry of NADPH being oxidized per actin residue being modified would not be expected as some H_2O_2 molecules would not react with actin side chains. The lack of a severing activity of MICAL supported by [32], who observed that monomers are released from the ends of the actin filament, would be also consistent with the observed time-course of NADPH oxidation in the presence of F-actin. With the reasonable assumption that MICAL recognizes a small region of the actin filament, a severing activity would lead to an increase of F-actin

fragments long enough to be recognized as MICAL substrates. Thus, NADPH oxidation should accelerate as the concentration of actin fragments increases over time. With a loss of monomers from the ends, the filaments concentration would remain essentially constant for a significant amount of time leading to the observed traces (Figure 12).

The precise site where MICAL MO binds to actin is not known, although there is consensus on the fact that G-actin does not stimulate NADPH oxidation. Accordingly, G-actin was not oxidized when incubated with NADPH and the human MICAL-1 forms [79]. The MO domain is sufficient to bring about the actin chemical modifications, *in vitro*, ruling out that the CH, LIM and C-terminal regions of MICAL determine the specificity of the reaction [78, 79]. In the model of mouse MICAL-1 MOCH in complex with F-actin proposed by [76] (Figure 11), MO apparently interacts with actin with the face where the NADPH binding site should be located. Upon "extraction", Met44 of the D-loop seems to occupy a position in front of the FAD isoalloxazine ring roughly corresponding to that of Trp400 in the crystallographic structures of various oxidized MICAL MO forms. Thus, actin and NADPH binding seem mutually exclusive events making it difficult to explain the activating effect of F-actin on the rate of NADPH oxidation, regardless of the reaction mechanism. In PHBH both p-hydroxybenzoate (pOHBz) and NADPH access the enzyme from the same side with pOHBz binding first. But pOHBz is a small molecule whose presence in the active site does not sterically interfere with NADPH binding and actually promotes the events that lead to flavin reduction and, eventually, the hydroxylation reaction. With the information available, it is difficult to conceive a model in which reduced and $NADP^+$-free MO (or a stable 4a-hydroperoxide intermediate) binds to F-actin and only at this stage it completes the catalytic cycle. Reduced MICAL-1 MO is rapidly reoxidized in the presence of oxygen and no intermediate indicating a stable 4-hydroperoxide or hydroxyl intermediate could be observed even in the stopped-flow (Vanoni and Vitali, unpublished). Furthermore, it would be difficult to explain how F-actin both accelerates the rate of MO reduction by NADPH [76-79] and lowers its K_m [78, 79]. The observation that MO reduction leads to the formation of a channel located on the opposite face of MO to the NADPH binding site ([64], Figure 4), and the suggestion of Siebold et al. [64] that this could be the face for MICAL-actin interaction would be consistent with the activating effect of F-actin on enzyme reduction by NADPH placing the actin and NADPH binding sites on opposite faces of MICAL. The channel that connects the protein surface to the active site, and other possible access points to the flavin through protein breathing motions, seems rather narrow. Thus, an amino acyl side chain could access the flavin and be modified, but also they may be the exit points of H_2O_2 produced by the NADPH oxidase activity of MICAL.

The differences between an oxidase and a monooxygenase reaction depend on the fine modulation of the stability of the 4-OOH intermediate, which may be very subtle [115-117].

Regardless of the mechanism adopted by MICAL in its F-actin depolymerizing activity, kinetic analyses can be useful to determine how F-actin enhances NADPH oxidation and which is the role played by the CH, LIM and C-terminal domain in modulating the reaction.

The apparent steady-state kinetic parameters of the reaction of human MICAL-1 forms in the presence of F-actin were studied by monitoring the initial velocity of NADPH oxidation spectrophotometrically in the F-actin stabilizing buffer (F-buffer, [78, 79], Table 3). In the absence of F-actin, due to the combination of the ionic strength and pH effects on MICAL forms, the $K_{m,\ NADPH}$ values measured in F-buffer are 5-20-fold higher than those measured in the standard assay buffer (20 mM Hepes/NaOH, pH 7.0), while the apparent k_{cat} for NADPH is only marginally reduced (Table 3). In the presence of F-actin (2.4 – 4.5 μM) the catalytic efficiency ($k_{cat}/K_{m,NADPH}$) of all species increased significantly due to both a drop of $K_{m,NADPH}$ values and an increase of k_{cat}. $K_{m,NADPH}$ reached value as low or lower than those measured in the low ionic strength standard assay buffer. (Table 3). Thus, the MO domain seems to have become insensitive to the presence of the additional domains upon binding to F-actin. Differences in the kinetic parameters among the various species should not be overinterpreted due to the intrinsic difficulty of this type of assays. The apparent k_{cat} values also increased 2-10-fold. By varying F-actin at NADPH concentrations that were 5-20-fold the observed $K_{m,NADPH}$ a hyperbolic increase of the initial velocity of the reaction was observed leading to the determination of an apparent K_m for F-actin of 3-5 μM (as measured in terms of monomer concentration) for MO, MOCH and MOCHLIM, supporting the proposal that MO bound to F-actin is essentially insensitive to the presence of the other domains. Accordingly, the k_{cat} for MO, MOCH and MOCHLIM reached similar values that were up to 10-fold higher than those measured in the standard buffer once the error associated with the determinations is taken into account, as well as the fact that a complete kinetic analysis was not performed due to the difficulty to precisely control the assay composition due to the use of F-actin, an intrinsically dynamic and heterogeneous substrate. With full-length human MICAL-1 the apparent $K_{m,F\text{-}actin}$ was 6-10-fold higher than that measured with the other forms (Table 3). It was interpreted to reflect the double equilibrium between the autoinhibited (inactive) and the fully active conformations, which lies towards the inactive form when full-length MICAL is free in solution (as estimated from the study of the NADPH oxidase activity) and that in which the protein in the active conformation binds F-actin with the same affinity as the other forms (Figure 14, [79]). Thus, it appeared that F-actin could be sufficient to stabilize the active conformation of MICAL by binding to the MO domain even in the absence of activators. However, the latter would promote F-actin depolymerization by increasing the local concentration of the MICAL form that is able to bind the filament. The effect would be a lowering of the apparent K_m for F-actin to the value measured with the isolated MO domain. Once the MICAL's MO domain is bound to actin, the affinity for NADPH drops and k_{cat} increases. McDonald and Palfey [77] nicely demonstrated that mouse MICAL-2 MO is reduced by NADPH approximately 100- fold faster in the presence of F-actin ($k_{red} \sim 8\ s^{-1}$ vs $0.074\ s^{-1}$) and that F-actin causes a 30 mV increase of the mid-point potential of MO-bound FAD from -240 mV to -212 mV. If the greater tendency of FAD to be reduced by NADPH were shown at the transition state for hydride transfer, it would justify the increase of k_{red} with mouse MICAL-2 MO and the 10-20-fold increase of k_{cat} with all human MICAL-1 forms.

The effect of F-actin on the steady-state kinetic parameters of mouse MICAL-1 MO and MOCH was also recently studied by varying NADPH concentration in the presence of different levels of F-actin [76] leading

to the conclusion that the CH domain has an important effect on the MICAL MO reaction in the presence of F-actin.

In these experiments actin appeared to behave as non-essential activator. Accordingly, the data were fitted based on the scheme depicted in Figure 15. F-actin had no effect on the $K_{m,NADPH}$ of MO, which remained constant (28. 85 ± 2.4 μM) at increasing F-actin concentrations, but lowered the corresponding value of MOCH (5-6 –fold from 37.7 ± 8.4 μM to 6 ± 1.8 μM). The increase of the apparent k_{cat} was lower on MICAL MO (4-5 - fold from 0.69 to 3.4 s^{-1}) than with MOCH (~7 fold from 1.66 ± 0.31 s^{-1} to 12.3 ± 1.5 s^{-1}). Furthermore, the K_d values for the complex between F-actin and the free oxidized MO or MOCH forms were calculated to be similar (9.3 ± 1.9 μM for MO and 10.5 ± 3.4 μM for MOCH). NADPH bound to MO had no effect on the affinity for F-actin, but the thermodynamic cycle of Figure 15 led to calculate a low dissociation constant of actin from the MOCH-NADPH complex (1.68 ±0.96 μM).

Thus, it was concluded that the CH domain plays an important modulatory role on the reaction of MICAL MO with F-actin supporting proposals made when only MICALs primary structures were available. The structure of mouse MICAL-1 MOCH, as well as the model of MOCH in complex with F-actin (Figure 11), do not predict interactions between the MO and CH domain [76]. Thus, intermolecular interactions between the CH domain of one MOCH monomer and the MO domain of another MOCH – only in the presence of F-actin - have been invoked to explain the different effects of F-actin on MO and MOCH [76]. In the crystal structure of MOCH, where the connection between MO and CH of the same molecule could not be seen, several possible mutual arrangements of the two domains were identified. Some of the conformations were ruled out by taking the account the length of the peptide connecting the MO and CH, one option was selected on the basis of SAXS measurements in solution (Figure 11). However, intermolecular interactions bringing the CH in contact with the MO domain are possible under conditions that would promote dimerization of MOCH, which has not been observed in solution yet.

These conclusions fully agree with the idea that the CH domain has an important modulatory role of the MICAL-actin interaction, but are in contrast with the data shown for the corresponding human MICAL-1 forms. In the light of the similarity between the human and mouse proteins this finding was unexpected, and a detailed analysis of the data available is worthwhile.

In the experiments with mouse MICAL-1 MO and MOCH, F-actin was correctly treated as a non-essential activator according to the scheme in Figure 15 because the rate of NADPH oxidation was significant in the explored NADPH concentration range also in the absence of F-actin. This is the first unexpected finding. In the absence of F-actin and in the high ionic strength F-actin stabilizing buffer (F-buffer) $K_{m,NADPH}$ values in the range of 29-40 μM for MO and MOCH were measured. These values are surprisingly low because of the effect of ionic strength on both mouse [63] and human [78, 79] MICAL-1 on this parameter (compare the values in Hepes and F-buffer in Table 3 for the human forms). A $K_{m,NADPH}$ of 222 μM was measured at pH 7 in the presence of 0.1 M NaCl for mouse MICAL-1 MO in the same lab [63]. The k_{cat} values (0.69 ± 0.02 s^{-1} for MO and 1.7 ± 0.5 s^{-1} for MOCH) seem also low compared to that

previously reported for MO from the same lab (77 s^{-1}, [63], even after recalculation leading to a value in the 4-5 s^{-1} range, see before) and those obtained with the human proteins (Table 3). With the human proteins the activity of each one of the MICAL forms in the absence of F-actin was negligible in the light of the high $K_{m,NADPH}$ in F-buffer in the absence of F-actin and both the drop of $K_{m,NADPH}$ and increase of k_{cat} in its presence (Table 3, [78, 79]). Thus, only the lower branch the scheme in Figure 15 would be operative. The analysis of the dependence of the reaction from NADPH concentration at different levels of F-actin was not done for the human proteins because of the difficulty to precisely control the reaction components under the experimental conditions, which appear to be similar to those adopted for the study of the mouse MO and MOCH forms.

Assuming that the $K_{m,NADPH}$ with mouse MO in the absence of F-actin was underestimated, but not that in the presence of F-actin, a drop in $K_{m,NADPH}$ could be caused by F-actin also for mouse MICAL-1 MO. With F-actin and both MO and MOCH, there is a good agreement between the $K_{m,NADPH}$ measured in F-buffer in the presence of 2-4 μM F-actin with the mouse (20-30 μM) and human species (11-50 μM) . It should be noted that in [76] NADPH was varied between 3 and 100 μM with MO. At the lowest NADPH concentration, the initial velocity, which is usually measured within the first 10% of the reaction to ensure the measurement of initial velocities, should have been calculated where the absorbance change was only 0.3 x 10^{-3} mM x 6.23 mM^{-1} cm^{-1} =0.001869 in 1 cm pathlength cells. The latter hypothesis can be made by comparing the traces of supplementary figure 4A for MO assays in the presence of 100 μM NADPH and different F-actin concentrations with the corresponding values of reaction velocity expressed as μM NADPH oxidized per second in panel C of the same figure [76]. For the corresponding measurements with MOCH, the NADPH concentration was varied between 10 and 150 μM so that the initial velocities of assays at the low NADPH concentration were also difficult to measure and true saturation with NADPH was not reached, at least in the absence of F-actin. The k_{cat} measured with MOCH in the absence of F-actin (1.7 $s^{-}1$) is similar to that measured with the corresponding human MICAL-1 form (Table 3), but the k_{cat} with MO (0.69 ± 0.02 s^{-1}) is 100-fold lower than that reported by the same laboratory before (77 s-1, [63]) and approximately 4-5-fold lower than that recalculated from the raw data shown in [63] and that measured with the human MICAL-1 MO (Table 3). The determination of protein concentration through the calculated extinction coefficient at 280 nm of the apoprotein could account for a 20-30 % overestimation of protein concentration, but this correction would not be sufficient to reconcile the data with the mouse and human MO's or between the previous and current data with the same mouse enzyme form. Interestingly, when one plots the k_{cat} values extrapolated at infinite NADPH concentration as a function of F-actin concentration using the data in Table 4 of [76] (reported in Figure 16), it seems that the lowest F-actin concentration has no activating effect on the k_{cat} of MO suggesting an interesting sigmoid behavior, which has not been discussed [76]. Unfortunately, F-actin concentrations between 0 and 2 μM have not been explored with mouse MOCH to further clarify this aspect [76]. With the human forms, deviations from a hyperbolic dependence of v/E from F-actin concentration at low F-actin concentrations have been looked for, but not detected. A sigmoid behavior could

have even been due to spontaneous dissociation of F-actin upon dilution to concentrations closer to that critical for filament formation.

Interestingly, if one disregards the k_{cat} values obtained in the absence of F-actin, the dependencies of k_{cat} on F-actin concentration with MO and MOCH follow the same hyperbolic trend with an apparent $K_{m,F\text{-}actin}$ of ~1 μM. The k_{cat} value calculated for MO in the presence of F-actin are also approximately 6-times lower than those calculated for MOCH (compare the left and right axes of Figure 16). If one made the hypothesis that 0.6 μM MO was used for the determination of k_{cat} in the absence of F-actin (as stated in the methods section) but 0.1 μM was actually used in the presence of F-actin (as in the legend of Supplementary figure S4, [76]), the k_{cat} values obtained at different F-actin concentrations for MO and MOCH would nicely overlap and both extrapolate to a maximum k_{cat} at infinite F-actin of ~12 s^{-1} (Figure 16), which would reduce the discrepancy with respect to the data obtained with the human proteins (Table 3). Comparison of the values in Table 4, Figure 8 and Panel D of Supplementary Figure S4 of [76], however, leads to a puzzling finding. The initial velocity values calculated for assays done with 0.1 μM MOCH in the presence of 100 μM NADPH and varying F-actin (Supplementary figure S4, panel D) are different from those shown in Figure 8 and in Table 4 (e.g.: at 8 μM F-actin the initial reaction velocity in panel D is 2.0 μM NADPH oxidized per second, which translates into a v/E of 20 s^{-1} for 0.1 μM enzyme in the assay (legend of Supplementary Figure S4) and 3.3 s^{-1} for 0.1 μM enzyme (methods, main text) *versus* a value of 8-10 s^{-1} read off the graph in Figure 8, main text).

Indeed, more work needs to be done with all forms of MICAL available to establish the precise effect of F-actin on the reaction of MICAL forms. Proper handling of F-actin solutions and carefully controlling the actual reaction composition, especially when F-actin is the varied substrate, probably are the critical issue.

Overall, there is consensus on the activating effect of F-actin and the time-course and extent of NADPH initially observed with the human and mouse MICAL-1, which leads to the proposal that MICAL disassembles F-actin through *in situ* H_2O_2 production via its NADPH oxidase activity.

Modulators of MICAL

Since the discovery of MICAL as a cytoplasmic multi-domain protein that is activated by semaphorin-bound plexin, it has been proposed that the enzyme exists in at least two conformations: the inactive conformation typical of the free enzyme and the active conformation, which is stabilized when MICAL interacts with plexin with its C-terminal region. The “autoinhibited” model of free MICAL was further substantiated by Schmidt et al. [41] who demonstrated that MICAL-1 forms lacking the C-terminal region were “constitutively active” in cells also leading to enhanced H_2O_2 production, and also that the C-terminal domain most likely interacts with the protein fragment comprising the MO, CH and LIM domains [41]. Thus, the inactive state of MICAL could be depicted as a “closed” conformation and the active one as an “open” conformation (Figure 17). The comparison of the kinetics of the NADPH oxidase activity of the

human MICAL1 forms leads to propose that the "closed" inactive conformation represents approximately 90% of the total protein in solution at neutral pH. Its amount may decrease at low pH as the acidic C-terminal region is titrated. The "open" conformation representing the active form should have a k_{cat} similar to that of the other forms (2-3 s^{-1}) and a $K_{m,NADPH}$ of ~ 0.5 mM, which may also be higher in the cell depending on the actual ionic strength and anion composition. Only MICAL in the open conformation may bind to F-actin through its MO domain. As a result F-actin could even be sufficient to shift the equilibrium towards its active form. The state of the filament depends on a variety of different factors so that it is also possible that a basal MICAL depolymerizing activity exists, but it is offset by prevailing filament polymerization as well as competition with one or more of the several actin binding proteins. Whether the "closed" and "open" MICAL forms can dimerize through the C-terminal domain (as observed for the RBD of MICAL-3) or other domains (e.g.: the LIM domain that stabilizes a MICAL-1 MOCHLIM dimer) still needs to be established.

Whether and how MICAL-1 interactors modulate its activity is an area of research that has just started to be explored. Also the search of small molecule inhibitors has been done only in a few cases, but with scarce success so far. However, interfering with MICAL activity with small molecules or peptide analogs that would either block the activity of MO or lock MICAL in an inactive conformation could be of great interest in the light of the variety of important biological functions in which it is involved.

Small molecule inhibitors of the NADPH oxidase activity of MICAL-MO.

The identification of selective inhibitors of MICAL MO may be important for the understanding of its mechanistic features and, on a longer run, for drug design.

(3)-epigallocatechin-3-O-gallate (EGCG) was proposed to be a selective MICAL MO inhibitor since it has been reported to inhibit PHBH [118] and it abolished the response of semaphorin A in dorsal root neurons more effectively than other antioxidants [2]. Indeed, Nadella et al. [63] observed strong inhibition of H_2O_2 production with mouse MICAL-1 MO in the coupled assay with HRP and Amplex red. EGCG behaved as a noncompetitive inhibitor with respect to NADPH and the calculated K_i was very low (2 μM). However, EGCG, as a catechol, is a potent H_2O_2 scavenger. Accordingly, by measuring the effect of EGCG on the NADPH oxidase activity of human MICAL-1 MO, as directly monitored by absorbance changes at 340 nm, EGCG was found to yield complex kinetic patterns and to be a more modest inhibitor (K_i, 17 μM, [78]). Low concentrations of EGCG caused no changes in MICAL MO spectrum, but protein aggregation/ denaturation was observed at concentrations above 25 μM, thus explaining the complex kinetics [78]. Furthermore, the observed inhibition of semaphorin signaling observed with cells may be due to effects other than a specific inhibition of MICAL. Recently, it was confirmed that EGCG stabilizes the actin network in retinal ganglion cells, but the experiments ruled out a direct involvement of semaphorin and MICAL inhibition in the process [119]. Interestingly, the structures of EGCG and of xanthofulvin (SM-216289) are related. The latter is a natural compound that has been shown to interfere with the semaphorin signaling pathway and to promote neurons regeneration following spinal cord injury in rats [120] and also in other models [121, 122]. Thus, it cannot be ruled out that their mechanism of action is somehow related. These

compounds may act as general scavengers of ROS or they may bind to one or more proteins and even induce changes like the aggregation/denaturation observed with MICAL. We have not been able to find studies on the direct effect of catechols or related compounds on actin, independent from their antioxidant activity, which might help to shed light on some of these observations.

On the basis of the similarity with PHBH, and assuming that MICAL MO could also be a hydroxylase oxidizing a protein side chain, several amino acids, peptides and benzoate derivatives were tested as effectors of the NADPH oxidase activity of human MICAL-1 MO [78]. Only benzoate derivatives had detectable effects behaving as competitive inhibitors with respect to NADPH. The K_i values decreased as the number of hydroxyl groups increased with a K_i of 0.1 mM for 2,4,6-trihydroxybenzoate.

Interestingly, a peptide mimicking the actin D loop (synthetic actin "D-loop" peptide, residues 39 to 52 of actin) was synthetized and used in co-crystallization experiments of mouse MICAL-1 MOCH [76]. No peptide was found in complex with MOCH in the resulting crystals [76]. Since no comments were specifically made in the paper, one should assume that the same peptide was tested as a mouse MICAL-1 MO or MOCH substrate or effector but no effect was detected.

It has also been proposed that CCG1423 inhibits MICAL-2 both in cells and the purified MOCH form [46]. CCG1423 belongs to a series of compounds that are of interest for cancer treatment. They have been proposed to be inhibitors of the Rho family of small GTPases, but their precise mechanism has not been actually clarified yet [46]. CCG1423 inhibited the reaction of MICAL-2 MOCH, as monitored at 340 nm, but only in the presence of F-actin. Accordingly, CCG1423 had no effect on the NADPH oxidase activity of human MICAL-1 MO and MOCH forms (Vitali and Vanoni, unpublished), while its interference with the activity in the presence of other human MICAL-1 forms and/or F-actin has not been studied yet.

Protein activators and inhibitors.

Several proteins have been found to interact with MICAL, such as the already mentioned CasL, the cytoplasmic side of Plexin A, Rab proteins, CRMP and NDR1/2. Studies on the effect of these proteins on the modulation of MICAL activities have been limited so far to CRMP and Rab proteins. However, the availability of several MICAL forms and the growing structural information on protein fragments, may soon lead to thorough studies also using purified proteins.

MICAL and CRMP.

CRMPs (from collapsin response mediator proteins) are among the first proteins that were discovered to mediate cytoskeleton collapse following semaphorin signaling. They promote microtubules formation by interacting with tubulin dimers, and they are inhibited by phosphorylation [21]. It was shown that MICAL interacts with several members of the CRMP family in the cell [41], and that their interaction is promoted by semaphorin binding to their plexin receptors. Furthermore, CRMP1 and MICAL-1 seemed to cooperate to promote COS7 cell collapse even in the absence of semaphorin stimulation. By co-immunoprecipitation

from extracts of cells in which various combinations of CRMP and MICAL forms had been expressed, the strongest interaction was observed between full-length MICAL and CRMP-1, but the MICAL MOCHLIM region seemed sufficient. Overexpression of MICAL-1 MOCH and MOCHLIM forms led to an increase of H_2O_2 production as measured in cell extracts in the presence of NADPH, HRP and Amplex Red. Co-expression of CRMP1 or addition of a C-terminally truncated (but native-like) CRMP1 form (residues 8-525) to extracts of cells expressing MICAL-1 MOCH or MOCHLIM quenched the NADPH-dependent H_2O_2 production suggesting that CRMP1 may be the substrate of the hydroxylase activity of MICAL-MO. Morinaka et al [42] and Gellert et al. [113, 116] reached the different conclusion that plexin-activated MICAL-1 may specifically promote the oxidation of Cys504 of CRMP2 through H_2O_2 production leading to CRMP2 dimerization through an intermolecular disulfide bridge. CRMP2 covalent dimers or the covalent complex between CRMP2-Cys504 and thioredoxin (or glutaredoxin) thiol would promote CRMP2 phosphorylation by GSK-3β (glycogen synthase kinase 3). Phosphorylation of CRMP2 would inhibit its activity and lead to microtubules disassembly. It should be noted that inspection of the sequences of CRMP from different classes shows that Cys 504 is present only in CRMP2. Thus, the results with CRMP1 [41] and CRMP2 [42] may not be in contrast.

The study of the interaction of human MICAL-1 forms with the same 8-525 CRMP1 form that led to quenching of the H_2O_2 produced by MICAL MOCH and MOCHLIM in cell extracts [41] was initiated in our laboratory (Vitali and Vanoni, unpublished) thanks to CRMP expressing plasmids kindly provided by Prof. Strittmatter (Yale University, USA). When equimolar amounts of human MICAL-1 MO or MOCH and CRMP1 (10 μM each) were mixed at low ionic strength, aggregation was observed with no indication of other perturbations of the MICAL MO spectrum. Dissociation was obtained by adding NaCl up to 0.1 mM indicating a non-specific electrostatic interaction. Accordingly, the NADPH oxidase activity of MICAL MO and MOCH was inhibited in a concentration dependent manner by CRMP1 at low ionic strength. Inclusion of increasing concentrations of NaCl in the assays relieved the inhibition. Interestingly, with 200 mM NaCl (MO) and 50-100 mM NaCl (MOCH) a small (10-20%) increase of activity was observed for CRMP concentrations up to 10-20 μM. At higher concentrations CRMP1 was again inhibitory. Mild activation followed by inhibition was also observed in the F-actin stabilizing buffer and with other MICAL forms. The increase of activity of MICAL MO and MOCH could be ascribed to a small $K_{m,NADPH}$ decrease. The interaction of MICAL MO and MOCH and CRMP1 was confirmed in the presence of F-actin in F-buffer. Here CRMP1 addition decreased the velocity of NADPH consumption by 10-20% and lost its effect at concentrations higher than 10-20 μM mirroring the trend observed in its absence. A K_d for the MICAL MO (or MOCH)/CRMP complex of 5-10 μM could be estimated from the kinetic data. A loose binding would be consistent with a modulatory role of CRMP-MICAL interaction. If one wanted to draw a scheme in which MICAL promotes microtubules disassembly by modulating CRMP activity, kinetic data would indicate that MICAL may function by physically sequestering CRMP1. In turn CRMP1 may promote H_2O_2 production by MICAL, but the stimulation would be very mild. However, CRMP would also compete – although very weakly - with MICAL for binding to the actin filaments somehow opposing cell collapse. These preliminary

studies tend to rule out that CRMP1 is a MICAL substrate or activator as observed for F-actin. However, they show that the availability of the series of well-characterized human MICAL-1 forms can help identifying and characterizing its effectors under controlled *in vitro* conditions.

MICAL and Rab.

Rab1 was shown to bind the C-terminal region of MICAL-1,-2, -3 in rat tissues and various cell lines [25, 26]. An extensive search of Rab interactors [123] demonstrated that MICAL-1 (but surprisingly not MICAL-2 and MICAL-3) and MICAL-like -1 and -2 proteins as well as MICAL-cL bind several proteins of the broad Rab family. They all bind Rab8A/B, Rab10, Rab13, and Rab15, which are phylogenetically similar, but only MICAL-1 bound Rab1A/B. This distribution suggested common (redundant) roles of various MICALs in intracellular membrane trafficking but assigned to MICAL-1 a function related to membrane-associated signaling. In independent studies MICAL-3 was also found to bind Rab6 and Rab8 [33].

Recently, Fremont et al . [32, 124] demonstrated that MICAL-1 is essential to complete cell division extending the number of essential processes in which MICAL-1 is involved and reinforcing the interest of MICAL as a drug target. Rab35, a member of the Rab1 family, was shown to both localize MICAL-1 in late cytokinetic bridges, and to activate its actin depolymerizing activity in the cell and in *in vitro* experiments on single actin filaments using microfluidics.

An extensive sequence analyses led Rai et al. [69] to find a set of human proteins (EHBP1 and EHBP1L1, C16orf45) sharing with MICAL-1, -3 , MICAL-L1, MICAL-L2 and MICAL-cL the C-terminal region that was structurally characterized as the Rab binding domain. The interaction of these regions with members of the Rab8 (Rab8, Rab10, Rab13 and Rab15) and Rab1 (Rab1a, Rab1 b, Rab35) families were studied by combining gel filtration chromatographies and isothermal titrations calorimetry. The various fragments RBD bound proteins of the Rab families with different stoichiometries and affinities, confirming possible *in vivo* differential control. Only one Rab1 molecule binds to MICAL-1 and MICAL-3 RBD with micromolar affinity (K_d, 2-3 µM), a result later confirmed by Fremont et al. [32] with Rab35 and MICAL-1 (K_d, 6-13 µM in a buffer with a triple ionic strength). Two molecules of Rab8 bound to the RBD of MICAL-1 and MICAL-3. The high affinity site (located towards the N-terminus) exhibited an affinity in the 30-50 nM range for the MICAL-1 and MICAL-3 RBDs, and the low affinity site a K_d 10-fold lower for MICAL-1 (~ 0.5 µM) than for MICAL-3 (4.4 µM).

A Rab binding site with a K_d in the nM range would suggest that Rab activation upon binding to GTP would recruit MICAL to the membrane where Rab is located. A looser interaction through the second Rab binding site would allow fine tuning of MICAL activity depending on the local activated Rab concentration and its changes over time [69]. That Rab35 activates human MICAL-1 towards actin depolymerization has been shown in single actin filament assays [32]. Ongoing work with the series of human MICAL-1 forms available in our lab is showing that indeed Rab8 (kindly provided by Drs Goody and Mueller, MPI, Dortmund) activates the NADPH oxidase activity of full-length MICAL-1, specifically increasing the observed k_{cat}, but has a mild effect on forms lacking the C-terminal domain.

How the MICAL regions preceding its RBD affect binding stoichiometries and affinity for Rab and how Rab8 alters the kinetics of MICAL-1 in the presence of F-actin and the postulated equilibrium between the inactive (closed) and active (open) MICAL conformations (Figure 17) is being studied.

Conclusions and future perspectives.

The interest in MICALs is steadily increasing because of the finding of their involvement of a variety of essential biological functions in neuronal and non-neuronal cells. Interfering with their activity and activation may be of broad therapeutic interest. In spite of the fact that structural and mechanistic information is available, MICAL's mechanism of action is still poorly understood. In particular, current literature leads to sometimes non univocal conclusions.

There is general agreement that the MICAL MO domain catalyzes a NADPH oxidase reaction and that the catalytic activity of the MO domain is essential for the unprecedented NADPH-dependent F-actin depolymerase activity of all MICAL forms. The NADPH oxidase activity of MICAL, which is limited by enzyme reduction by NADPH, may be physiologically relevant depending of activating signals and local NADPH concentration.

A great deal of work has been done to clarify the mechanism of F-actin depolymerization with two prevailing views. According to several results, MICAL MO switches from a NADPH oxidase (in the free state) to a specific actin Met44 and Met47 hydroxylase generating the R stereoisomer of methionine sulfoxide. This activity of MICAL is at the origin of the incorrect definition of MICAL as a methionine sulfoxide oxidase that appears in the annotations found in databanks.

Met44 and Met47 modification would destabilize the filament and eventually lead to release modified actin monomers, which could be repaired by R-specific methionine sulfoxide reductases in the cell. MICAL-dependent oxidation of actin residues would destabilize the fragment and make it more susceptible to the cofilin disassembly action, and possibly also alter the function of other actin binding proteins. At the time of writing, the Protein Data Bank contains an unreleased structure (5UBO) of gelsolin in complex with MICAL-oxidized actin, suggesting that a cooperative effect was also found between MICAL and this important regulator of actin cytoskeleton.

Other results indicate that MICAL MO always catalyze a NADPH oxidase reaction, which is enhanced when it binds to F-actin through a significant increase of k_{cat} and decrease of $K_{m,NADPH}$. H_2O_2 released *in situ* by MICAL-MO could modify several actin residues at or near the interface between actin monomers with a destabilizing effect on the actin filament and, eventually, release of modified monomers (Figure 13). The extent and type of modifications would depend on the precise geometry of the complex between MICAL-MO and F-actin.

An argument against the hypothesis that F-actin modification is mediated by *in situ* release of H_2O_2 is the low reactivity of methionyl residues with hydrogen peroxide and the lack of effect of up to 40 mM H_2O_2 on

filament depolymerization [32, 71, 113]. The presence of DTT (typically 1 mM) in the F-actin stabilizing buffer is not sufficient to explain the lack of effect of such a high H_2O_2 concentration. However, it appears that the sensitivity of actin filaments to H_2O_2 greatly varies as a function of its precise status. For example, Lassing et al. [125] studied the H_2O_2-induced modification of cysteinyl residues in various G- and F-actin forms. With respect to F-actin, they showed that high H_2O_2 (20 mM) disassembles the filament with release of monomers (which can be monitored as a decrease of solution viscosity – in general - and also of fluorescence, when pyrenyl-actin is used) but only causes fragmentation (as monitored by the decrease of solution viscosity, but not fluorescence) at a lower concentration (5 mM). Furthermore, removal of calcium ions below 1 μM appeared to make the filament insensitive to H_2O_2. No methionine oxidation was reported in these experiments, a finding that may be consistent with the low reactivity of methionine side chain with H_2O_2 discussed by Manta and Gladyshev [113] who report a second order rate constant for methionine oxidation by H_2O_2 of ~10^{-2} M^{-1} s^{-1}. While the precise environment may strongly alter the methionine thioether reactivity, it should be noted that release of H_2O_2 from the enzyme active site through a NADPH oxidase activity may generate impressively high local product concentrations. For example, with a naif calculation, if one takes into account the Avogadro number (6.022×10^{23} molecules/mol), the presence of just one molecule of H_2O_2 (1.66×10^{-24} mol) in a cube of 1 nm side (volume = $(1 \times 10^{-9})^3$ m^3 x 10^3 l/m^3 = 1 x 10^{-24} l) corresponds to a H_2O_2 concentration of 1.66 M. For these reasons, further work is certainly needed to clarify the details of MICAL mechanism of actin filament disassembly. Unfortunately, carrying out the reaction in the presence of $^{18}O_2$, and monitoring ^{18}O incorporation in actin or release as water would not clarify the mechanism as the same result would be expected for a H_2O_2-mediated or a direct hydroxylation reaction, namely: one oxygen atom would be incorporated in the oxidized actin residue and the other in a water molecule.

MICAL was proposed to severe F-actin as the first disassembly event [70, 71, 73], but recent data [32] showed that actin monomers are released from the filaments' ends progressively shortening them. Filaments disassembly seems in all cases slower than their modification by MICAL [32, 73] explaining the peculiar time-course of fast NADPH oxidation that exceeded the amount of actin present (Figure 12) and is in contrast with the notion that MICAL MO acts as a specific Met44 and Met47 hydroxylase, but supports that actin disassembly is mediated by H_2O_2 production.

Whether it will be possible to correlate the kinetic properties of MICAL in solution with information derived from direct observation of MICAL effect on individual actin filaments as in the microfluidics set-up shown in Fremont et al. [32] is not known, but it would be extremely interesting. Unfortunately, the fluorescence of FAD bound to MICAL MO is strongly quenched [78] so that direct observation of MICAL in action, at the single molecule level, does not seem straightforward. High resolution electron microscopy approaches may indeed help establishing how MICAL forms bind to F-actin and clarifying if F-actin actually

leads to MO activation even in the absence of ligands bound to other domains. The approach has been successfully applied to several actin binding proteins (see, e.g.: [111, 126-128]).

Unfortunately, the availability of the structures of the MO, CH and C-terminal RBD of MICALs has not yet clarified whether MICAL MO always catalyzes a NADPH oxidase activity or if it switches to a monooxygenase reaction when actin-bound. The model of mouse MICAL-1 MOCH in complex with F-actin does not seem to be compatible with the observation that MICAL MO should simultaneously bind F-actin and NADPH to explain the activating effect of F-actin on the NADPH oxidation reaction (Figure 11). Very subtle differences distinguish monooxygenases and oxidases, and inspection of the MICAL MO active site is not sufficient to provide clear-cut answers. It would be actually very interesting to definitely prove that MICAL is an NADPH oxidase, which exploits the PHBH scaffold and the associated conformational flexibility for fine control of the reaction. Such conformational flexibility could actually be simply required to promote the interaction with the actin filament, which is conformationally heterogeneous [129].

How the MICAL's domains that follow MO modulate the catalytic activities also needs to be established. This issue is biologically relevant being linked to the *in vivo* regulation of MICAL activity. Only the C-terminal region seems to have a clear role in stabilizing an inactive form of MICAL, which appears in equilibrium in solution with a fully active species. Whether the C-terminal RBD binds directly to the MO domain (perhaps preventing NADPH binding or the conformational changes that must take place during the catalytic cycle) or the other MICAL domains are important has not been clarified yet. The experiments of Schmidt et al. [41] would argue that the entire MOCHLIM fragment is required. Accordingly, the inhibitory effect of the MICAL-1 RBD on single actin filaments depolymerization was verified with a MICAL-1 MOCHLIM form [32]. However, experiments with the different purified MICAL forms in solution would allow to determine stoichiometries and binding strength. Several proteins of the Rab family have been shown to bind to MICALs' C-terminal RBD yielding 2:1 or 1:1 complexes depending on the Raba md MICAL RBD couple. That Rab binding to MICAL activates the protein has been shown by microfluidics observing the acceleration of degradation of individual actin filaments by full-length MICAL1 in the presence of Rab35, and also by us, studying the effect of Rab on the NADPH oxidase reaction of the full-length and truncated human forms (unpublished). Whether proteins other than Rab that interact with MICAL's C-terminal region stabilize the active "open" form of MICAL, and therefore, increase the NADPH oxidase activity will also need to be explored. The identification of the binding sites of each one of the MICAL's interactors, as well as the study of how they alter the catalytic properties of the various enzyme forms may provide valuable information.

Even if the mechanism of MICAL-catalyzed reactions and their control is far from being understood, there are sufficient information, methods and materials to develop selective inhibitors that could also serve to clarify structure-functions relations of MICAL in a synergistic way.

Acknowledgments

The contribution of past and present members of the laboratory to published and ongoing work and of several colleagues for helpful discussions is gratefully acknowledged.

Table 1. Summary of general properties of human MICAL-1 forms

	MO	MOCH	MOCHLIM	MICAL
Mass (calculated[a])	55000	68338	86348	118920
Mass (experimental[b])	54915	68222	87615	119084
pI (calculated [a])	9.1	7.7	6.7	6.2
$\lambda_{max, Vis (native)}$	458	458	458	458
$\lambda_{max, UV (native)}$	276	276	278	278
UV/Vis[c]	10.2	15.5	16.1	19
ε_{458}[d], $mM^{-1}cm^{-1}$	7.9 ± 0.1	8.0 ± 0.2	8.3 ± 0.2	7.9 ± 0.7
$\varepsilon_{280, apoprotein}$[e], $mM^{-1}cm^{-1}$	68.87	89.84	99.81	124.79
$\varepsilon_{280, holoprotein}$[f], $mM^{-1}cm^{-1}$	89.87	110.84	120.81	145.79
$\varepsilon_{280, holoprotein}/\varepsilon_{280, apoprotein}$	1.3	1.23	1.21	1.17
$\varepsilon_{280, denatured}$[g], $mM^{-1}cm^{-1}$	91.57	112.54	122.51	147.49

[a]Mass calculated with the Compute pI/mw tool at www.expasy.ch by taking into account the post-translational removal of the starting Met residue. [b]Mass determined by MALDI-TOF. [c]Ratio of the absorbance values at 276 or 278 nm and those at 458 nm of purified protein preparations (up to 9 determinations; the associated error was less than 3%, [79]). [d]The extinction coefficient of FAD bound to the native proteins and the FAD content was determined by either TCA or guanidine denaturation of the proteins (2-4 independent determinations, [79]). The values are similar to that previously measured with MO (8.1 ± 0.2 $mM^{-1}cm^{-1}$, 7 determinations, [78]), which, for practical purposes, is used to quantify all human MICAL-1 forms. [e]Calculated for the apoprotein using the Protparam tool at www.expasy.ch by assuming that all Cys residues are reduced. [f]Calculated by adding the experimental extinction coefficient of FAD at 280 nm in diluted buffer at pH 7.0 (21 $mM^{-1}cm^{-1}$) to the calculated extinction coefficient of the apoprotein (previous row). [g]Calculated by adding the experimental extinction coefficient of FAD at 280 nm of FAD in 3 M guanidine/HCl in diluted buffer, pH 7.0 (22.7 $mM^{-1}cm^{-1}$) to the calculated extinction coefficient of the apoprotein.

Table 2. Summary of the access code of the structures of MICAL fragments deposited in the Protein Data Bank.

PDB ID	Protein	Method	Resolution, Å	Ref.
2BRA	Mouse MICAL-1 MO	MX	2	[63]
2BRY	Mouse MICAL-1 MO	MX	1.45	[64]
C2C4	Mouse MICAL-1 MO, NADPH-reduced	MX	2.9	[64]
4TXI	Mouse MICAL-1 MOCH	MX	2.31	[76]
4TXK	Mouse MICAL-1 MOCH	MX	2.88	[76]
2DK9	Human MICAL-1 CH	NMR	N/A	[83]
2E9K	Human MICAL-2 CH	NMR	N/A	-
2D88	Human MICAL-3 CH	NMR	N/A	-
1WYL	Human MICAL-1 CH as CH domain of NEDD9 interacting protein with CH and LIM domains	NMR	N/A	-
2CO8	Human MICAL-1 LIM as LIM domain of NEDD9 interacting protein with CH and LIM domains	NMR	N/A	-
5LE0	Human MICAL-1 Rab binding domain	MX	3.3	[32]
5LPN	Human MICAL-1 Rab binding domain in complex with Rab10	MX	2.8	[69]
5SZG	Human MICAL-3 Rab binding domain	MX	2.7	[69]
5SZH	Human MICAL-cL in complex with Rab1b	MX	2.3	[69]
5SZI	Human MICAL-cL in complex with Rab8a	MX	2.85	[69]
5SZJ	Human MICAL-cL in complex with Rab10	MX	2.66	[69]
5SZK	Human MICAL-cL in complex with Rab1bR8N	MX	2.8	[69]

-, no accompanying publication

Table 3. *Steady-state kinetic parameters of the NADPH oxidase reaction catalyzed by human MICAL-1 forms.* Assays were carried out in 20 mM Hepes/KOH buffer, pH 7 (Hepes), or in F-buffer (9.5 mM Tris/HCl, pH 7.7, 45 mM KCl, 0.18 mM $CaCl_2$, 0.18 mM $MgCl_2$, 1.1 mM ATP, 1.3 mM DTT) in the presence of the indicated NADPH and F-actin concentrations or concentration ranges at 25°C. Apparent k_{cat} and K_{NADPH} values and their associated errors were determined by fitting the data to the Michaelis-Menten equation. The values have been taken from [78, 79]

Buffer	Protein nM	NADPH μM	F-actin μM	k_{cat} s^{-1}	K_m μM	k_{cat}/K_m $s^{-1}mM^{-1}$
Hepes	MO, 20	10-300	-	3.1 ± 0.1	19 ± 2	163 ± 18
	MOCH, 60	10-600	-	2.5 ± 0.1	134 ± 5	18.5 ± 1
	MOCHLIM, 60	30-1000	-	3.5 ± 0.1	230 ± 16	15.3 ± 1.2
	MICAL, 690	100-800	-	0.28 ± 0.01	375 ± 33	0.75 ± 0.07
F-buffer	MO, 120[a]	10-300	-	2.6 ± 0.4	555 ± 118	4.6 ± 1.2
	MO, 20[a]	10-300	2.4	12 ± 0.5	11.3 ± 2.7	1090 ± 260
	MO, 20[a]	300	7 - 35	20 ± 1.0	4.7 ± 1.0	4149 ± 908
	MOCH, 190	10-500	-	1.7 ± 0.1	459 ± 66	3.8 ± 0.6
	MOCH, 3	10-200	4.2	21 ± 1.2	50 ± 8	423 ± 72
	MOCH, 3	200	1 - 26	26 ± 1.2	2.7 ± 0.4	9487 ± 1468
	MOCHLIM, 125	25-1000	-	4.3 ± 0.2	966 ± 66	4.5 ± 0.4
	MOCHLIM, 12	20-200	4.4	6.4 ± 0.2	14 ± 1.6	448 ± 52
	MOCHLIM, 12	200	2-24	15 ± 0.6	4.4 ± 0.5	3390 ± 378
	MICAL, 1250	100-700	-	0.8 ± 0.5[a]	4652 ± 3202[a]	0.17 ± 0.15[a]
	MICAL, 91	10-400	4.3	1.9 ± 0.1	29 ± 5	64.8 ± 12.2
	MICAL, 91	200	3.8-23	7.8 ± 1.2	29 ± 7	276 ± 87

[a]the parameters are poorly defined due to the high K_m value for NADPH.

Figure 1. Domain organization in MICALs and general scheme of the reaction mechanism of flavin-dependent monooxygenases. Panel A. The location of domains in human MICAL-1, -2, -3 and in drosophila MICAL (D-MICAL) is shown. Color code: MO, monooxygenase-like domain, residues 1-489, yellow; CH, calponin homology domain, 510-613, cyan; LIM, 688-756, fuchsia; P, proline-rich region containing the PXXP signature (in bold) for binding to Src-homology domain-3 (SH3) domains, 829-P**PPKP**PR-835, orange; E, Glu-rich region, residues 866-880 in MICAL-1, which is more extended in MICAL-3 being between residue 910 and 1052, red; RBD, Ras binding domain identified by [32, 69] in the region originally proposed to form coiled-coils also named bMERB from the bivalent MICAL/EHBP Rab binding domain [69], residues 918-1067. In MICAL-2 light grey bars indicate regions that may also form helical structures according to previous sequence comparisons [62]. The potential nuclear localization signals of MICAL-2 (residues 660-681) and MICAL-3 (residues 663-683, [46]) are shown in dark purple. For this and the following figures, please refer to the on-line version for the color scheme. Panel B: A simplified scheme of the reaction mechanism of flavin-dependent monooxygenases that shows how the NAD(P)H-reduced flavin coenzyme can react with molecular oxygen and form a 4a-hydroperoxide intermediate, which evolves to yield oxidized flavin and hydrogen peroxide in the oxidase reaction or the hydroxylated substrate (SOH) in the monooxygenase activity. Production of superoxide is also possible, but has not been implicated in the case of MICAL.

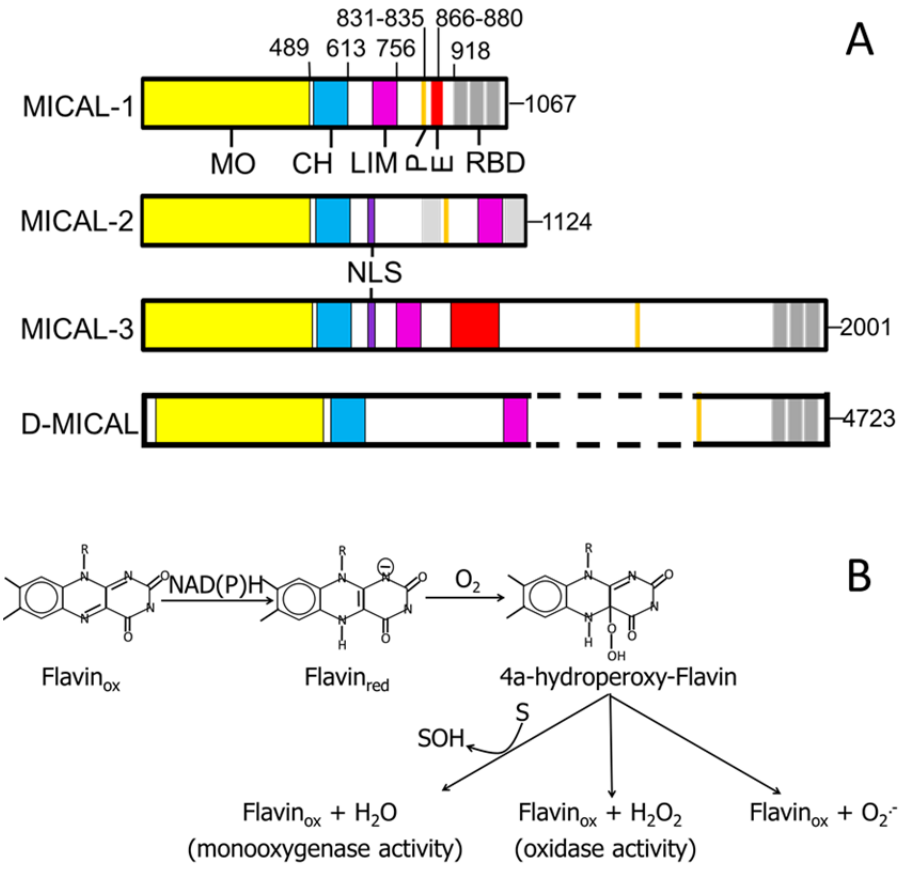

Figure 2. Absorption spectrum of human MICAL-1.

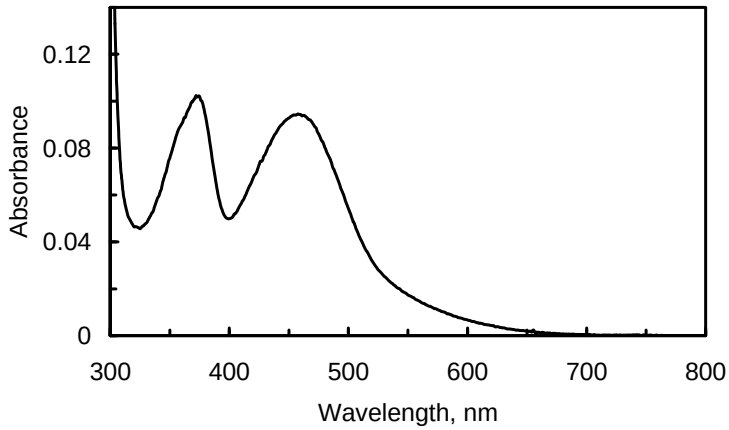

Figure 3. Comparison of the structures of the mouse MICAL-1 MO in the oxidized and reduced forms. The structures of the mouse MICAL-1 MO in the "as isolated" (oxidized, PDB ID: 2BRY, panels A and B, [64]) and NADPH-reduced (2C4C, panels C and D, [64]) forms are shown in two orientations. The circle in panels A and C indicates the approximate position of conserved surface residues in the 1-85 subdomain that form a patch of basic potential (see also Figure 4). In panels B and D the protein is viewed from the NADPH binding site, as identified by similarity with PHBH. Color code: MO domain: 1-85, blue; 86-227, 374-444 and 235-366 in different shades of grey; β9 (227-233) and β15 (367-373), light green; the conserved 395-405 loop is in red. FAD and Trp400 are also in cylinders. Carbon atoms are shown in green, nitrogen in blue and oxygen in red. This and all the other figures representing structural models were generated with CCP4MG [130].

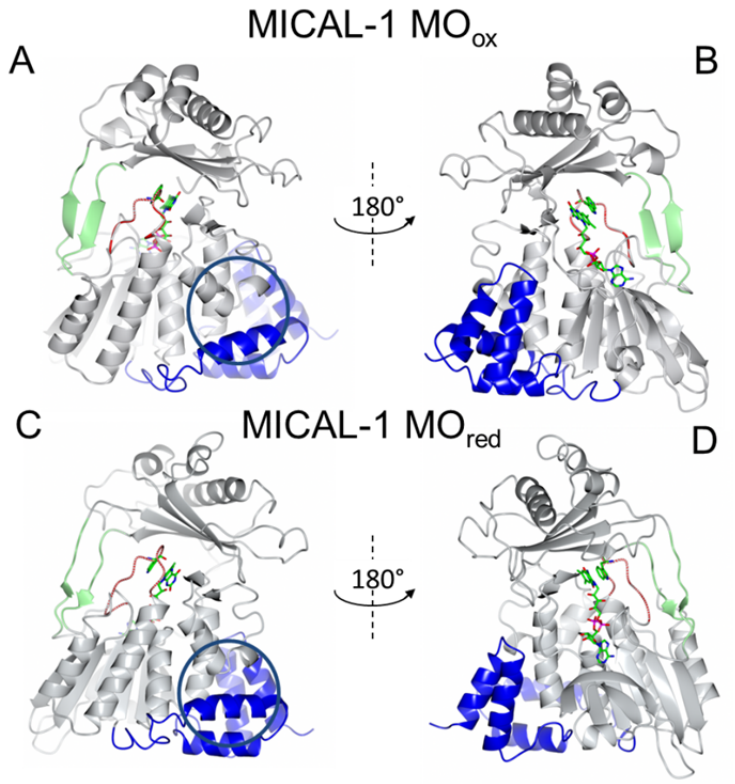

Figure 4. Comparison of the surface charge and FAD accessibility of the mouse MICAL-1 MO in the oxidized and reduced forms. The surface charge of the mouse MICAL-1 MO in the "as isolated" (oxidized, PDB ID: 2BRY, panels A and B, [64]) and NADPH-reduced (2C4C, panels C and D, [64]) forms are shown in the same orientations as in Figure 3. FAD is shown in cylinders. Carbon atoms are shown in green, nitrogen in blue and oxygen in red. The circle shows the patch of positive potential on one face of the protein; the white star indicates the conserved basic residues that identify the NADPH binding site by similarity with PHBH. In Panel C, FAD is now exposed to solvent due to the opening of the channel described by [64] upon reduction. The rectangle marks the areas that have been blown up in the right panels indicated with the primed letters.

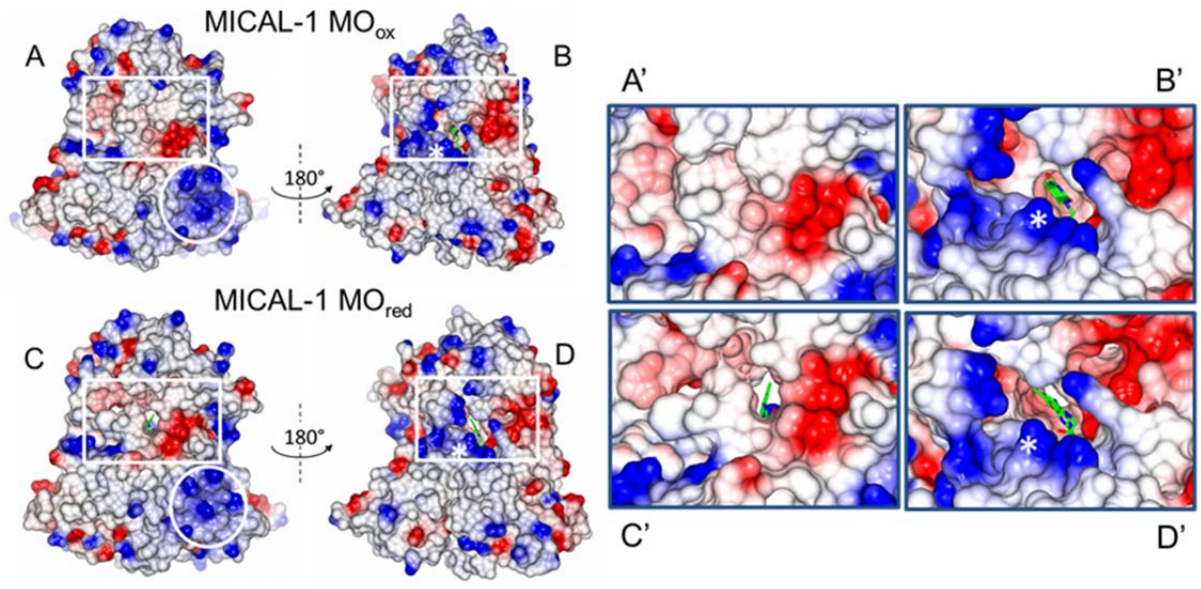

Figure 5. Interaction of FAD in MICAL MO oxidized (flavin out) and NADPH-reduced (flavin in) state. Selected residues surrounding FAD have been extracted from the structures of "as isolated" (2BRY) and NADPH-reduced (2C4C) mouse MICAL-1 MO ([64]). Potential hydrogen bonds (< 3.5 Å) are in grey.

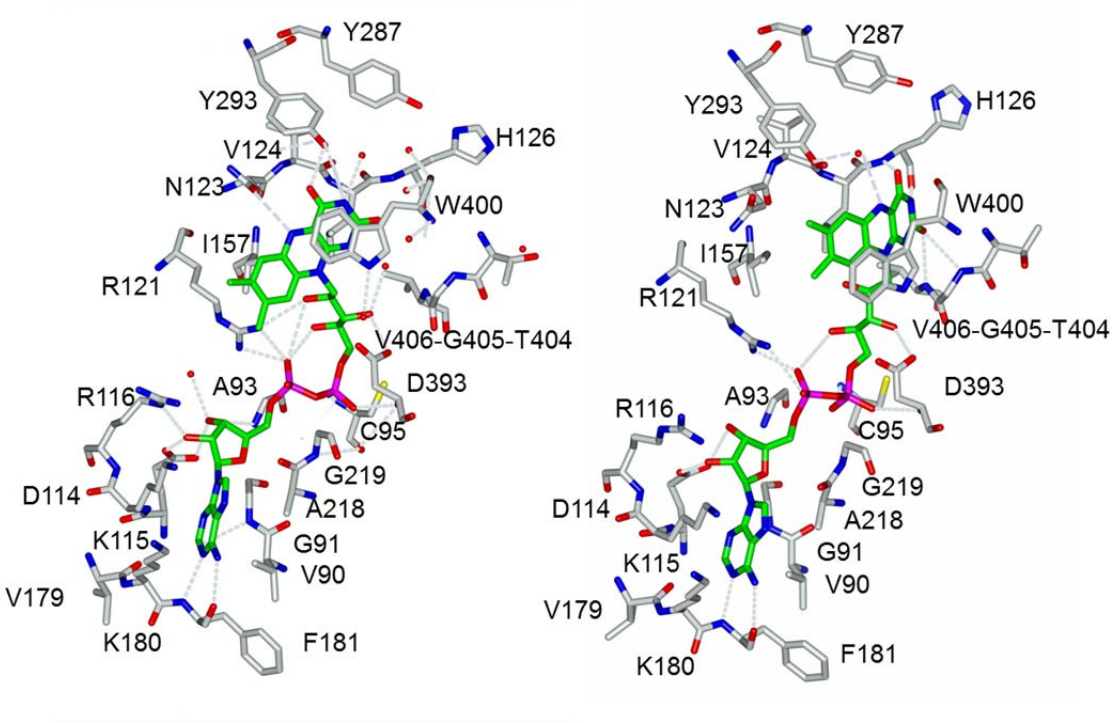

Figure 6. Structure of the mouse MICAL-1 MOCH fragment. The structure of the mouse MICAL-1 MOCH (PDB ID: 4TXI, [76]) is shown in two orientations as in Figure 3. Color code: MO domain: 1-85, blue; 86-227, 374-444 and 235-366, grey; β9 (227-233) and β15 (367-373) strands, light green; the conserved 395-405 loop is in red. CH domain: 507-614, cyan; conserved residues corresponding to the actin binding site are shown as cylinders with carbon atoms in grey; those of the potential PIP2 binding site are in cylinders with carbon atoms in green. FAD and Trp400 are also in cylinders. Carbon atoms are shown in green, nitrogen in blue and oxygen in red.

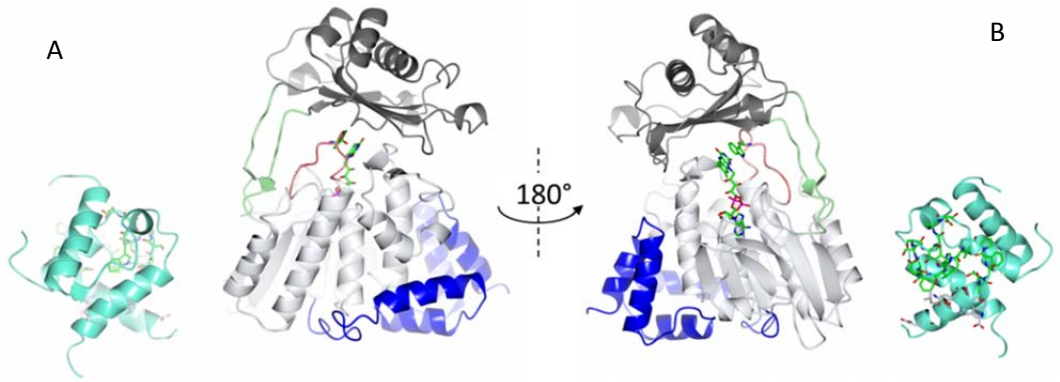

Figure 7. The CH and LIM domains of MICAL-1. Left panel. Details of the CH domain of mouse MICAL-1 (4TXI, [76]) highlighting the possible actin binding site (ABS, cyan) and the PIP2 binding site (PIP2) based on the similarity with type 2 CH domains. Residues matching the ABS and PIP2 binding site fingerprints are shown in cylinders. The region corresponding to the PIP2 binding site of type 2 CH domains is shown in worm representation in sea green. Right panel: model of the human MICAL-1 LIM domain. Since the structure was determined by NMR (2C08) a single chain model was obtained with Swiss-Model [131] and the sequence of human MICAL-1. The residues interacting with the zinc ions (spheres, red) are shown in cylinders.

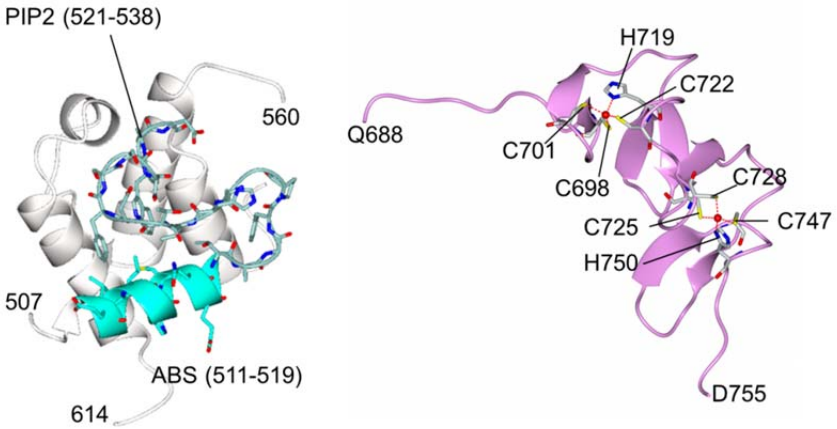

Figure 8. Structure of the Rab binding domain of human MICAL-1 and MICAL-3. Left: model of the human MICAL-1 Rab binding domain (ribbons) in complex with two copies of Rab10 (worms and tubes, grey, [69]). Some of the residues implicated in Rab10 binding [69] and those that were found to be essential for binding with Rab35 [32] are indicated in cylinders. Color code: ice, residues 918-993; light green, residues 994-1059. Right: model of the human MICAL-3 Rab binding domain, which forms a dimer in the crystal [69]. The residues corresponding to those implicated in Rab10 interaction in the MICAL-1/Rab10 structure are in cylinders to show how the interface between the MICAL-3 RBD monomers overlaps with the C-terminal Rab10 binding site of MICAL-1. The first and second half of the domain are shown as for MICAL-1 in ice and light green, respectively. Some residues are labeled to help orientation.

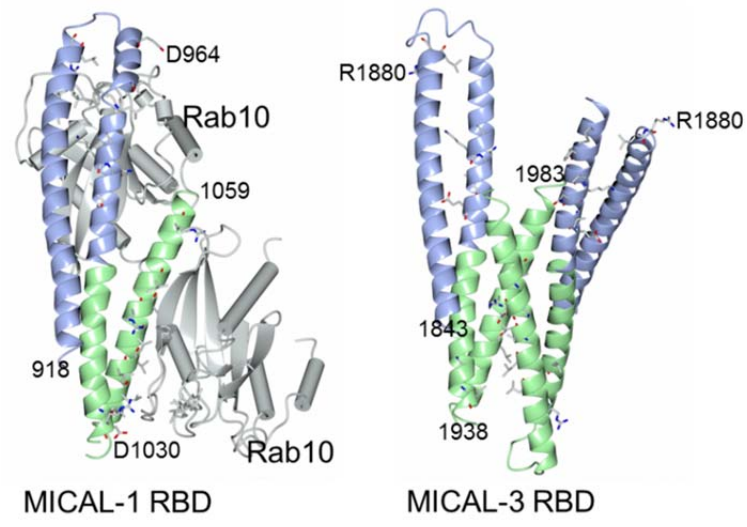

Figure 9. Sequence of the Rab binding domain of MICAL-1. Sequence of the 918-1067 region of human MICAL-1 highlighting the similarity between its N- and C-terminal halves as the result of a genetic duplication [69]. The regions corresponding to helices-1 (underline), -2 (double underline), and -3 (dotted underline) are shown along with residues that initially led to proposed the presence of a coiled-coil (grey highlight, [62]), some of the residues interacting with Rab10 (bold, [69]) and those that abolish or weaken interaction with Rab35 when mutated (blue, [32]).

```
918                                                                 993
KEEEMKRFCKAQTIQRRLNEIEAALRELEAEGVKLELALRR--------QSSSPEQQKKLWVGQLLQLVDKKNSLVAEEAELMI

                          994                                                 1067
                          TVQELNLEEKQWQLDQELRGYMNREENLKTAADRQAEDQVLRKLVDLVNQRDALIRFQEERRLSELALGTGAQG
```

Figure 10. pH dependence of the steady-state kinetic parameters of the NADPH oxidase reaction catalyzed by human MICAL-1 forms. The steady-state kinetic parameters k_{cat}, k_{cat}/K_{NADPH} and K_{NADPH} for the NADPH oxidase activity of human MICAL-1 and of the MO, MOCH, MOCHLIM truncated forms were determined spectrophotometrically at 25°C by varying NADPH concentration in a mixed buffer composed of 10 mM acetate, 5 imidazole, 5 mM Tris, (Buffer 1, ionic strength 10 mM (open circles) or of 12.5 mM formate, 5 mM imidazole, 5 mM Tris (Buffer 2, ionic strength 12.5 mM, closed circles). The curves were drawn with the equations and parameters values reported in [79]. The apparent pK_a values are shown in the figure. For clarity only the the pK_a obtained with MO in Buffer 1 are shown. The figure is reprinted from [79] with permission from the publisher.

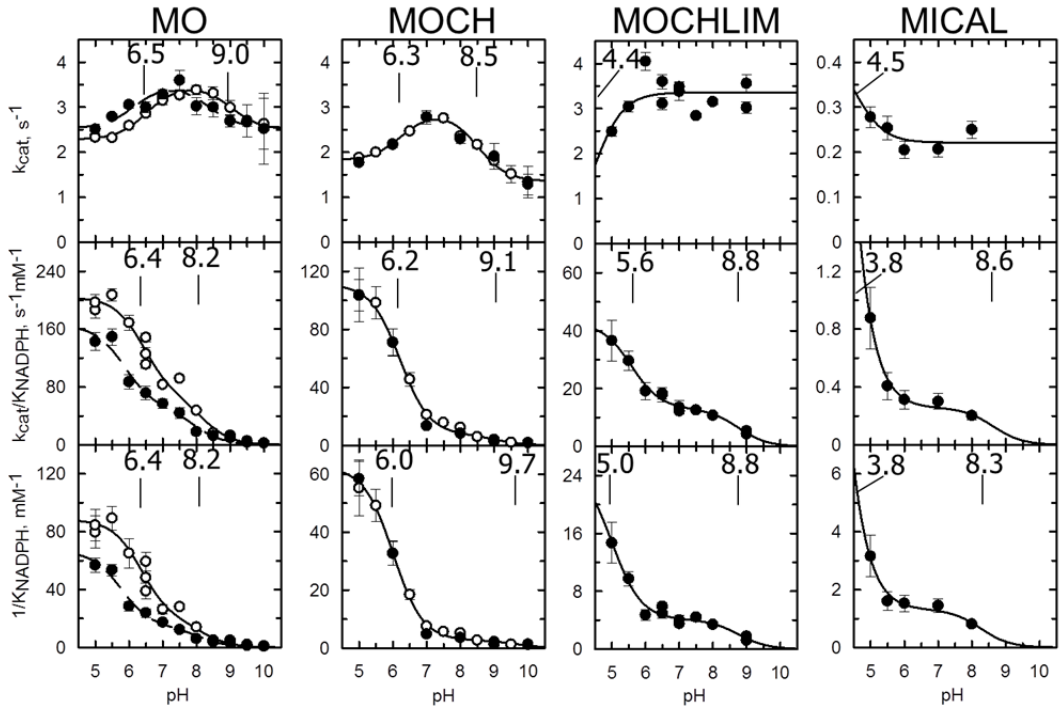

Figure 11. Model of mouse MICAL-1 MOCH in complex with actin Met44. Panels A -D depict the complex between mouse MICAL-1 MOCH (gold ribbons) and a fragment of an actin filament built by Alqassim et al. [76]. The MICAL MOCH was positioned placing the CH domain where the α-actinin CH1 domain binds to F-actin (dashed red line in A, dark green in B) so that the "large opening" of MO (i.e.: the NADPH binding site) was towards the filament according to the MOCH structure (Figure 6B). In a series of molecular dynamics simulations Met44 (sticks in C and D) of one actin subunit (green) was progressively constrained to reach a distance of approximately 3 Å from FAD 4a position as described by [76]. For comparison Panel E and F have been drawn using the mouse MICAL-1 MOCH structure (4TXI, [76]) and highlighting the N-terminal 1-85 region (blue), the β9 and β 15 strands connecting the FAD and the cap domain (dashed green), the 395-405 loop (dashed red), FAD (cylinders, carbon atoms cyan) and Trp400 (carbon atoms green). The distance between FAD-N5 and Trp400 CZ3 (which appears to occupy a position similar to that of Met44 in Panel D) is indicated in F. Note that in the "flavin in" conformation, the same Trp carbon atom may be roughly in front of FAD C9 of the dimethylbenzene ring (see Figure 5). The figures in A-D are reprinted from [76]with permission from the publisher.

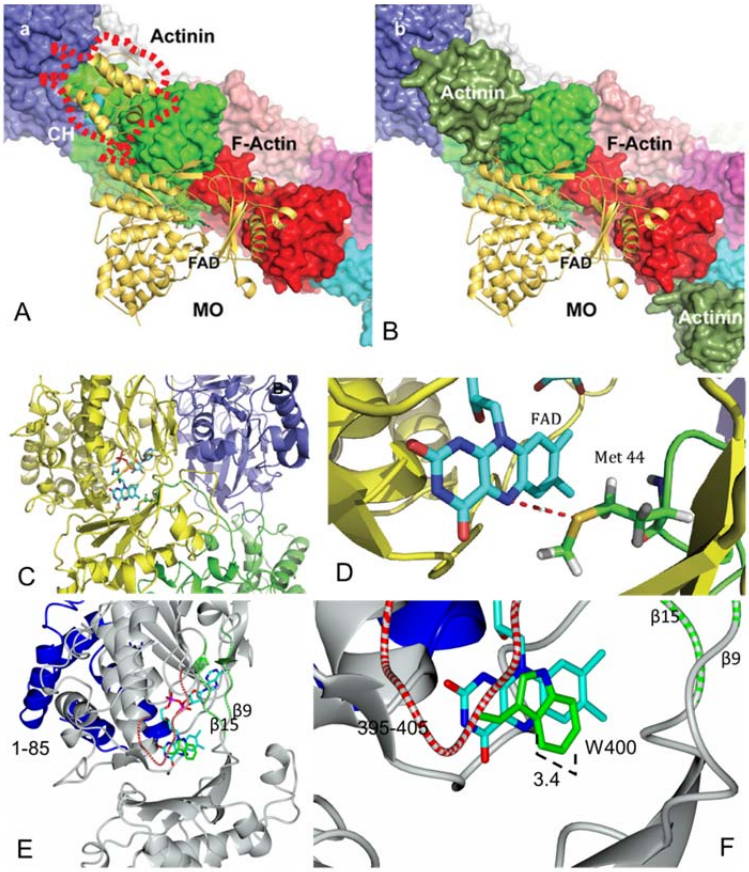

Figure 12. Effect of F-actin on the time-course and extent of NADPH oxidation catalyzed by human MICAL1 forms. MOCH (150 nM), MOCHLIM (115 nM), and full-length MICAL (1.5 μM) were incubated with NADPH (100 μM) in the absence (open circles) or in the presence of F-actin (5 μM, closed circles) in F-actin stabilizing buffer at 25 °C. The traces obtained with MO are similar to those shown for MOCH. The time-course of NADPH oxidation was monitored continuously by absorption spectroscopy at 340 nm. Reprinted from [79] with permission from the publisher.

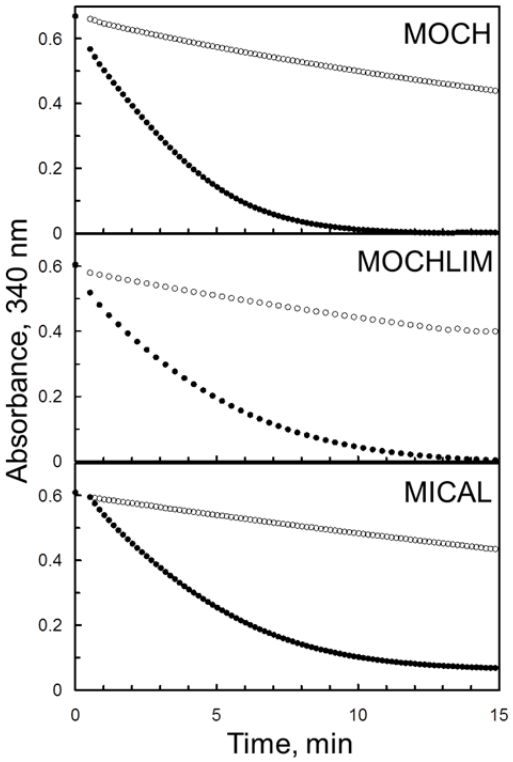

Figure 13. MICAL-1 modified actin residues. The residues that were found to be modified with similar probability in F-actin that had been treated with human MICAL-1 in [79] are shown in spacefill on the actin filament structure from PDB file 3J8I [111]. A detail is shown on the right. 2-3 actin residues were found to be modified in each monomer. Met44 and Met47, Met269 or Met283, Met355 or Trp340 or Trp 356, Met82 or Trp79 or Trp86 (in spacefill representation) were modified with the same probability.

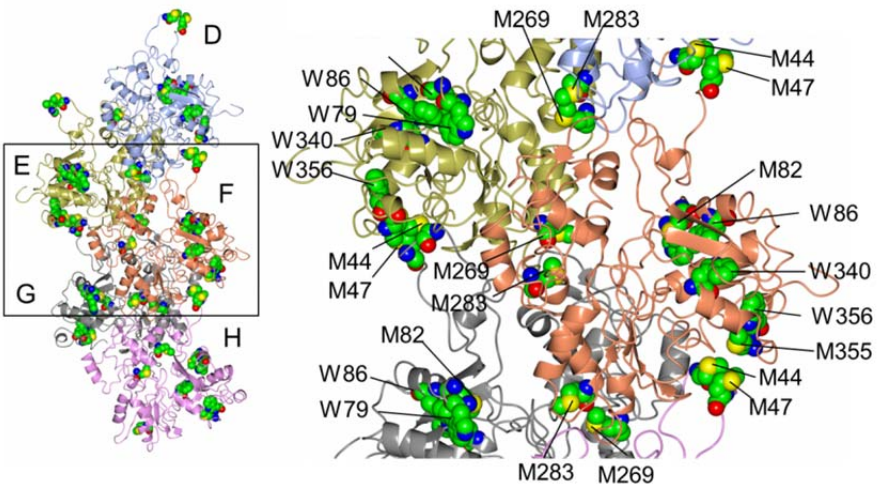

Figure 14. Proposed model of interaction between MICAL-1 in the active conformation and F-actin. The scheme explains the apparent K_m value for F-actin with full length human MICAL-1, which is approximately 10-fold higher than that measured with the other MICAL forms (see Table 3). The figure is reprinted from [79] with permission from the publisher.

$$\begin{array}{c} K_{eq} \sim 0.1 \\ MICAL_{inactive} \rightleftharpoons MICAL_{active} \\ K_d \sim 3\text{-}5\ \mu M \\ MICAL_{active} + F\text{-}actin \rightleftharpoons MICAL_{active} \bullet F\text{-}actin \\ \hline K_{d,\,app} \sim 30\text{-}50\ \mu M \\ MICAL_{inactive} + F\text{-}actin \rightleftharpoons MICAL_{active} \bullet F\text{-}actin \end{array}$$

Figure 15. Kinetic scheme of the activating effect of F-actin on the NADPH oxidoreductase reaction of MICAL MO. The scheme depicts the activating effect of F-actin on the activity of MICAL MO and MOCH proposed by [76] in which F-actin is treated as non-essential activator of MO reaction (see e.g.: [132]). In the thermodynamic scheme, K_1 is the dissociation constant of the enzyme/NADPH complex; K_2 is that of the enzyme F-actin complex. α is the factor by which F-actin modifies the K_d of the enzyme/NADPH complex: for no effect of actin on NADPH binding, α =1; for enhancement of binding α<1; for weakened binding α>1. As a consequence in the thermodynamic cycle in the scheme, binding of F-actin to the enzyme/NADPH complex is also modified by α. β is the factor that expresses the effect of F-actin on the reaction rate. For an acceleration of the reaction, β >1. According to the model proposed by ([76]) for the reaction of mouse MICAL-1 MO and MOCH both branches of the scheme are operative in the presence of F-actin, which has a different effect on MICAL-1 MO and MOCH. With MO, the data obtained by varying NADPH concentration at different F-actin levels were fitted with K_1 =28.85 ± 2.4 μM; K_3 = 9.3 ± 1.9 μM; α = 1; k_{cat} = 0.069 ± 0.02 s^{-1}; β = 4.7 ± 0.5. The corresponding data with mouse MICAL-1 MOCH were fitted with K_1 =37.7 ± 8.4 μM; K_3 = 10.5 ± 3.4 μM; α = 0.16 ± 0.04; k_{cat} = 1.66 ± 0.13 s^{-1}; β = 7.43 ± 0.31. For human MICAL-1 forms only the lower branch of the scheme would be operative in the presence of F-actin (Table 3).

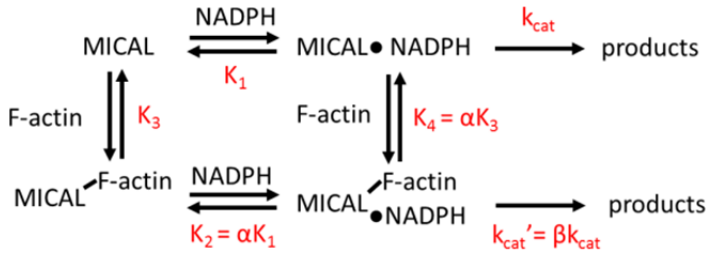

Figure 16. Effect of F-actin on the kinetics of mouse MICAL-1 MO and MOCH. The values of apparent k_{cat} for mouse MICAL-1 MO (circles, left axis) and MOCH (squares , right axis) extrapolated at infinite NADPH concentration in the presence of fixed F-actin levels were taken from Table 4 of [76] and plotted as a function of the stated F-actin concentration. The curve shows the fit to the Michaelis-Menten equation of the values obtained with MOCH in the presence of 2-8 μM F-actin. The Grafit program (Erythacus Software Ltd, UK) was used. The calculated values for the steady-state kinetic parameters were: k_{cat}, 11.7 ± 0.9 s^{-1}; $K_{m,F\text{-}actin}$, 0.9 ± 0.4 μM. The large error associated with the K_m value is due to the use of only three F-actin concentrations that are not suitably spaced to define the apparent K_m in the light of its low value. The plot shows how the apparent k_{cat} values measured with MO and MOCH in the presence of F-actin differ by a factor of ~6 but follow the same hyperbolic trend. See text.

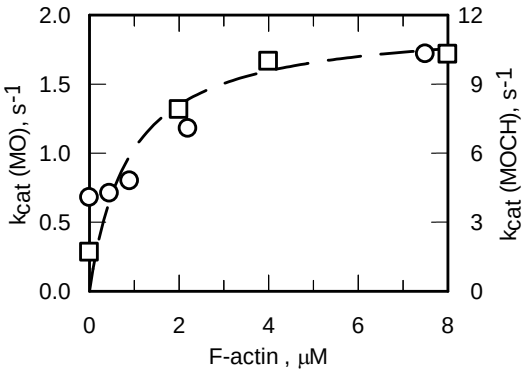

Figure 17. Proposed model of the equilibria among "autoinhibited" and active conformations of MICAL. The "autoinhibited" conformation of MICAL-1 is depicted as a "closed" form in equilibrium with the active "open" conformation. The equilibrium between the forms is shifted towards the open form by activating proteins that bind to the C-terminus (e.g.: the cytoplasmic side of plexin or Rab) or elsewhere. Binding of MO to F-actin (not to scale in the figure) would be sufficient to stabilize the active (open) form. The interaction between F-actin and MICAL that has been activated upon complex formation with plexin or other proteins is not shown for clarity. The possibility that the MICAL active/inactive conformations are further stabilized by dimerization should not be disregarded. Thus, dimerization of the species is indicated with a question mark The color code is the same as that in Figure 1A.

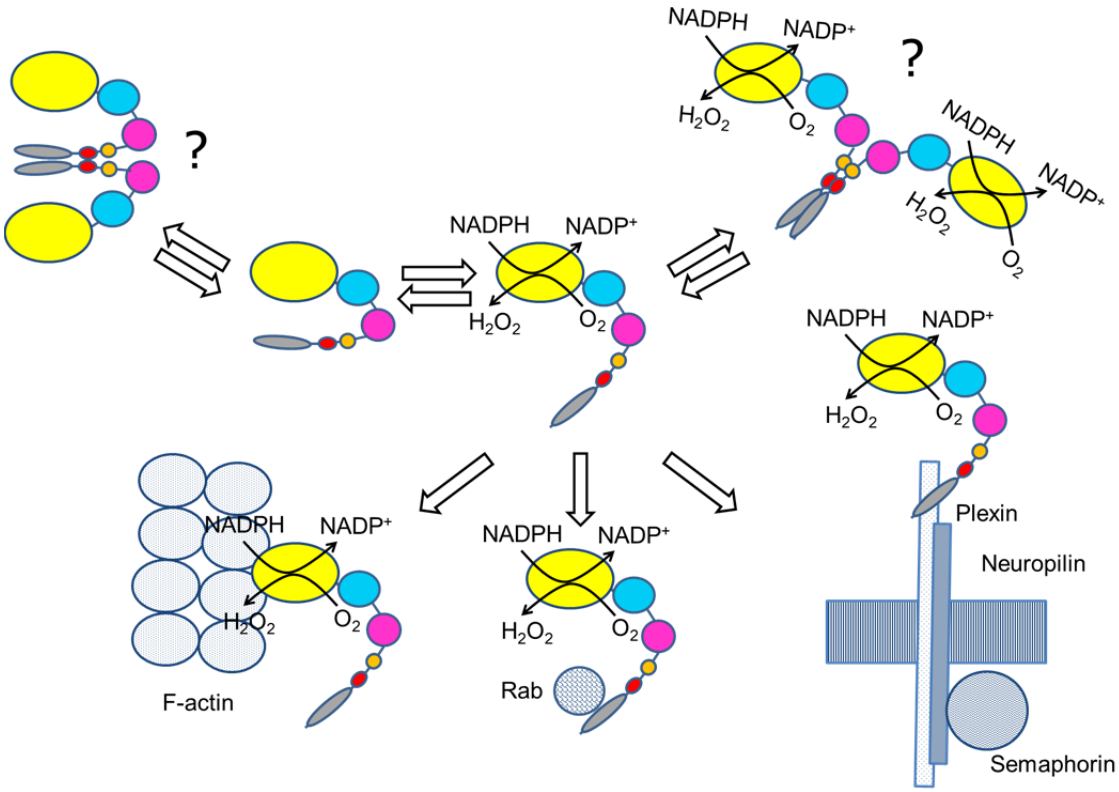

References

[1] Suzuki, T., Nakamoto, T., Ogawa, S., Seo, S., Matsumura, T., Tachibana, K., Morimoto, C., Hirai, H., MICAL, a novel CasL interacting molecule, associates with vimentin, The Journal of biological chemistry 277(17) (2002) 14933-14941.
[2] Terman, J.R., Mao, T., Pasterkamp, R.J., Yu, H.H., Kolodkin, A.L., MICALs, a family of conserved flavoprotein oxidoreductases, function in plexin-mediated axonal repulsion, Cell 109(7) (2002) 887-900.
[3] Tikhmyanova, N., Little, J.L., Golemis, E.A., CAS proteins in normal and pathological cell growth control, Cellular and molecular life sciences : CMLS 67(7) (2010) 1025-1048.
[4] Nikonova, A.S., Gaponova, A.V., Kudinov, A.E., Golemis, E.A., CAS proteins in health and disease: an update, IUBMB life 66(6) (2014) 387-395.
[5] Shagisultanova, E., Gaponova, A.V., Gabbasov, R., Nicolas, E., Golemis, E.A., Preclinical and clinical studies of the NEDD9 scaffold protein in cancer and other diseases, Gene 567(1) (2015) 1-11.
[6] Zhang, S.S., Wu, L.H., Roles of neural precursor cell expressed, developmentally downregulated 9 in tumor-associated cellular processes (Review), Mol Med Rep 12(5) (2015) 6415-6421.
[7] Kolodkin, A.L., Tessier-Lavigne, M., Mechanisms and molecules of neuronal wiring: a primer, Cold Spring Harbor perspectives in biology 3(6) (2011) a001727.
[8] Pasterkamp, R.J., Kolodkin, A.L., Semaphorin junction: making tracks toward neural connectivity, Current opinion in neurobiology 13(1) (2003) 79-89.
[9] Yazdani, U., Terman, J.R., The semaphorins, Genome biology 7(3) (2006) 211.
[10] Zhou, Y., Gunput, R.A., Pasterkamp, R.J., Semaphorin signaling: progress made and promises ahead, Trends in biochemical sciences 33(4) (2008) 161-170.
[11] Pasterkamp, R.J., Giger, R.J., Semaphorin function in neural plasticity and disease, Current opinion in neurobiology 19(3) (2009) 263-274.
[12] Kumanogoh, A., Marukawa, S., Suzuki, K., Takegahara, N., Watanabe, C., Ch'ng, E., Ishida, I., Fujimura, H., Sakoda, S., Yoshida, K., Kikutani, H., Class IV semaphorin Sema4A enhances T-cell activation and interacts with Tim-2, Nature 419(6907) (2002) 629-633.
[13] Takegahara, N., Kumanogoh, A., Kikutani, H., Semaphorins: a new class of immunoregulatory molecules, Philosophical transactions of the Royal Society of London. Series B, Biological sciences 360(1461) (2005) 1673-1680.
[14] Tamagnone, L., Giordano, S., Semaphorin pathways orchestrate osteogenesis, Nature cell biology 8(6) (2006) 545-547.
[15] Casazza, A., Fazzari, P., Tamagnone, L., Semaphorin signals in cell adhesion and cell migration: functional role and molecular mechanisms, Adv Exp Med Biol 600 (2007) 90-108.
[16] Valdembri, D., Regano, D., Maione, F., Giraudo, E., Serini, G., Class 3 semaphorins in cardiovascular development, Cell adhesion & migration 10(6) (2016) 641-651.
[17] Li, Z.X., Hao, J., Duan, X., Wu, N., Zhou, Z.K., Yang, F., Li, J., Zhao, Z.H., Huang, S.S., The Role of Semaphorin 3A in Bone Remodeling, Front Cell Neurosci 11 (2017) 40.
[18] Alto, L.T., Terman, J.R., Semaphorins and their Signaling Mechanisms, Methods Mol Biol 1493 (2017) 1-25.
[19] Derijck, A.A., Van Erp, S., Pasterkamp, R.J., Semaphorin signaling: molecular switches at the midline, Trends in cell biology 20(9) (2010) 568-576.
[20] Kolk, S.M., Pasterkamp, R.J., MICAL flavoprotein monooxygenases: structure, function and role in semaphorin signaling, Adv Exp Med Biol 600 (2007) 38-51.
[21] Schmidt, E.F., Strittmatter, S.M., The CRMP family of proteins and their role in Sema3A signaling, Adv Exp Med Biol 600 (2007) 1-11.
[22] Hung, R.J., Terman, J.R., Extracellular inhibitors, repellents, and semaphorin/plexin/MICAL-mediated actin filament disassembly, Cytoskeleton (Hoboken) 68(8) (2011) 415-433.
[23] Zhou, Y., Gunput, R.A., Adolfs, Y., Pasterkamp, R.J., MICALs in control of the cytoskeleton, exocytosis, and cell death, Cellular and molecular life sciences : CMLS 68(24) (2011) 4033-4044.

[24] Pasterkamp, R.J., Getting neural circuits into shape with semaphorins, Nature reviews. Neuroscience 13(9) (2012) 605-618.
[25] Weide, T., Teuber, J., Bayer, M., Barnekow, A., MICAL-1 isoforms, novel rab1 interacting proteins, Biochemical and biophysical research communications 306(1) (2003) 79-86.
[26] Fischer, J., Weide, T., Barnekow, A., The MICAL proteins and rab1: a possible link to the cytoskeleton?, Biochemical and biophysical research communications 328(2) (2005) 415-423.
[27] Beuchle, D., Schwarz, H., Langegger, M., Koch, I., Aberle, H., Drosophila MICAL regulates myofilament organization and synaptic structure, Mechanisms of development 124(5) (2007) 390-406.
[28] Friedberg, F., Alternative splicing for members of human mosaic domain superfamilies. I. The CH and LIM domains containing group of proteins, Molecular biology reports 36(5) (2009) 1059-1081.
[29] Rahajeng, J., Giridharan, S.S., Cai, B., Naslavsky, N., Caplan, S., Important relationships between Rab and MICAL proteins in endocytic trafficking, World journal of biological chemistry 1(8) (2010) 254-264.
[30] Cai, B., Xie, S., Caplan, S., Naslavsky, N., GRAF1 forms a complex with MICAL-L1 and EHD1 to cooperate in tubular recycling endosome vesiculation, Frontiers in cell and developmental biology 2 (2014) 22.
[31] Giridharan, S.S., Cai, B., Naslavsky, N., Caplan, S., Trafficking cascades mediated by Rab35 and its membrane hub effector, MICAL-L1, Communicative & integrative biology 5(4) (2012) 384-387.
[32] Fremont, S., Hammich, H., Bai, J., Wioland, H., Klinkert, K., Rocancourt, M., Kikuti, C., Stroebel, D., Romet-Lemonne, G., Pylypenko, O., Houdusse, A., Echard, A., Oxidation of F-actin controls the terminal steps of cytokinesis, Nature communications 8 (2017) 14528.
[33] Grigoriev, I., Yu, K.L., Martinez-Sanchez, E., Serra-Marques, A., Smal, I., Meijering, E., Demmers, J., Peranen, J., Pasterkamp, R.J., van der Sluijs, P., Hoogenraad, C.C., Akhmanova, A., Rab6, Rab8, and MICAL3 cooperate in controlling docking and fusion of exocytotic carriers, Current biology : CB 21(11) (2011) 967-974.
[34] Nishimura, N., Sasaki, T., Identification and characterization of JRAB/MICAL-L2, a junctional Rab13-binding protein, Methods in enzymology 438 (2008) 141-153.
[35] Rahajeng, J., Giridharan, S.S., Cai, B., Naslavsky, N., Caplan, S., MICAL-L1 is a tubular endosomal membrane hub that connects Rab35 and Arf6 with Rab8a, Traffic 13(1) (2012) 82-93.
[36] Sakane, A., Honda, K., Sasaki, T., Rab13 regulates neurite outgrowth in PC12 cells through its effector protein, JRAB/MICAL-L2, Molecular and cellular biology 30(4) (2010) 1077-1087.
[37] Sharma, M., Giridharan, S.S., Rahajeng, J., Caplan, S., Naslavsky, N., MICAL-L1: An unusual Rab effector that links EHD1 to tubular recycling endosomes, Communicative & integrative biology 3(2) (2010) 181-183.
[38] Sun, Y., Jaldin-Fincati, J., Liu, Z., Bilan, P.J., Klip, A., A complex of Rab13 with MICAL-L2 and alpha-actinin-4 is essential for insulin-dependent GLUT4 exocytosis, Molecular biology of the cell 27(1) (2016) 75-89.
[39] Zahraoui, A., MICAL-like1 in endosomal signaling, Methods in enzymology 535 (2014) 419-437.
[40] Ioannou, M.S., Bell, E.S., Girard, M., Chaineau, M., Hamlin, J.N., Daubaras, M., Monast, A., Park, M., Hodgson, L., McPherson, P.S., DENND2B activates Rab13 at the leading edge of migrating cells and promotes metastatic behavior, The Journal of cell biology 208(5) (2015) 629-648.
[41] Schmidt, E.F., Shim, S.O., Strittmatter, S.M., Release of MICAL autoinhibition by semaphorin-plexin signaling promotes interaction with collapsin response mediator protein, The Journal of neuroscience : the official journal of the Society for Neuroscience 28(9) (2008) 2287-2297.
[42] Morinaka, A., Yamada, M., Itofusa, R., Funato, Y., Yoshimura, Y., Nakamura, F., Yoshimura, T., Kaibuchi, K., Goshima, Y., Hoshino, M., Kamiguchi, H., Miki, H., Thioredoxin mediates oxidation-dependent phosphorylation of CRMP2 and growth cone collapse, Science signaling 4(170) (2011) ra26.
[43] Zhou, Y., Adolfs, Y., Pijnappel, W.W., Fuller, S.J., Van der Schors, R.C., Li, K.W., Sugden, P.H., Smit, A.B., Hergovich, A., Pasterkamp, R.J., MICAL-1 is a negative regulator of MST-NDR kinase signaling and apoptosis, Molecular and cellular biology 31(17) (2011) 3603-3615.
[44] Kirilly, D., Gu, Y., Huang, Y., Wu, Z., Bashirullah, A., Low, B.C., Kolodkin, A.L., Wang, H., Yu, F., A genetic pathway composed of Sox14 and Mical governs severing of dendrites during pruning, Nature neuroscience 12(12) (2009) 1497-1505.

[45] Rumpf, S., Bagley, J.A., Thompson-Peer, K.L., Zhu, S., Gorczyca, D., Beckstead, R.B., Jan, L.Y., Jan, Y.N., Drosophila Valosin-Containing Protein is required for dendrite pruning through a regulatory role in mRNA metabolism, Proc Natl Acad Sci U S A 111(20) (2014) 7331-7336.
[46] Lundquist, M.R., Storaska, A.J., Liu, T.C., Larsen, S.D., Evans, T., Neubig, R.R., Jaffrey, S.R., Redox modification of nuclear actin by MICAL-2 regulates SRF signaling, Cell 156(3) (2014) 563-576.
[47] Guillou, F., Roger, E., Mone, Y., Rognon, A., Grunau, C., Theron, A., Mitta, G., Coustau, C., Gourbal, B.E., Excretory-secretory proteome of larval Schistosoma mansoni and Echinostoma caproni, two parasites of Biomphalaria glabrata, Molecular and biochemical parasitology 155(1) (2007) 45-56.
[48] Dumas, A., Le-Bury, G., Marie-Anais, F., Herit, F., Mazzolini, J., Guilbert, T., Bourdoncle, P., Russell, D.G., Benichou, S., Zahraoui, A., Niedergang, F., The HIV-1 protein Vpr impairs phagosome maturation by controlling microtubule-dependent trafficking, The Journal of cell biology 211(2) (2015) 359-372.
[49] Loria, R., Bon, G., Perotti, V., Gallo, E., Bersani, I., Baldassari, P., Porru, M., Leonetti, C., Di Carlo, S., Visca, P., Brizzi, M.F., Anichini, A., Mortarini, R., Falcioni, R., Sema6A and Mical1 control cell growth and survival of BRAFV600E human melanoma cells, Oncotarget 6(5) (2015) 2779-2793.
[50] Pasterkamp, R.J., Verhaagen, J., Semaphorins in axon regeneration: developmental guidance molecules gone wrong?, Philosophical transactions of the Royal Society of London. Series B, Biological sciences 361(1473) (2006) 1499-1511.
[51] Rizzolio, S., Tamagnone, L., Semaphorin signals on the road to cancer invasion and metastasis, Cell adhesion & migration 1(2) (2007) 62-68.
[52] Meyer, L.A., Fritz, J., Pierdant-Mancera, M., Bagnard, D., Current drug design to target the Semaphorin/Neuropilin/Plexin complexes, Cell adhesion & migration 10(6) (2016) 700-708.
[53] Ashida, S., Furihata, M., Katagiri, T., Tamura, K., Anazawa, Y., Yoshioka, H., Miki, T., Fujioka, T., Shuin, T., Nakamura, Y., Nakagawa, H., Expression of novel molecules, MICAL2-PV (MICAL2 prostate cancer variants), increases with high Gleason score and prostate cancer progression, Clinical cancer research : an official journal of the American Association for Cancer Research 12(9) (2006) 2767-2773.
[54] Mariotti, S., Barravecchia, I., Vindigni, C., Pucci, A., Balsamo, M., Libro, R., Senchenko, V., Dmitriev, A., Jacchetti, E., Cecchini, M., Roviello, F., Lai, M., Broccoli, V., Andreazzoli, M., Mazzanti, C.M., Angeloni, D., MICAL2 is a novel human cancer gene controlling mesenchymal to epithelial transition involved in cancer growth and invasion, Oncotarget 7(2) (2016) 1808-1825.
[55] Deng, W., Wang, Y., Gu, L., Duan, B., Cui, J., Zhang, Y., Chen, Y., Sun, S., Dong, J., Du, J., MICAL1 controls cell invasive phenotype via regulating oxidative stress in breast cancer cells, BMC cancer 16 (2016) 489.
[56] Pasterkamp, R.J., Dai, H.N., Terman, J.R., Wahlin, K.J., Kim, B., Bregman, B.S., Popovich, P.G., Kolodkin, A.L., MICAL flavoprotein monooxygenases: expression during neural development and following spinal cord injuries in the rat, Mol Cell Neurosci 31(1) (2006) 52-69.
[57] Schmidt, E.R., Pasterkamp, R.J., van den Berg, L.H., Axon guidance proteins: novel therapeutic targets for ALS?, Progress in neurobiology 88(4) (2009) 286-301.
[58] Luo, J., Xu, Y., Zhu, Q., Zhao, F., Zhang, Y., Peng, X., Wang, W., Wang, X., Expression pattern of Mical-1 in the temporal neocortex of patients with intractable temporal epilepsy and pilocarpine-induced rat model, Synapse 65(11) (2011) 1213-1221.
[59] Giridharan, S.S., Rohn, J.L., Naslavsky, N., Caplan, S., Differential regulation of actin microfilaments by human MICAL proteins, Journal of cell science 125(Pt 3) (2012) 614-624.
[60] Giridharan, S.S., Caplan, S., MICAL-family proteins: Complex regulators of the actin cytoskeleton, Antioxidants & redox signaling 20(13) (2014) 2059-2073.
[61] Li, C., Gonsalves, C.S., Eiymo Mwa Mpollo, M.S., Malik, P., Tahara, S.M., Kalra, V.K., MicroRNA 648 Targets ET-1 mRNA and is cotranscriptionally regulated with MICAL3 by PAX5, Molecular and cellular biology 35(3) (2015) 514-528.
[62] Vanoni, M.A., Vitali, T., Zucchini, D., MICAL, the flavoenzyme participating in cytoskeleton dynamics, International journal of molecular sciences 14(4) (2013) 6920-6959.
[63] Nadella, M., Bianchet, M.A., Gabelli, S.B., Barrila, J., Amzel, L.M., Structure and activity of the axon guidance protein MICAL, Proc Natl Acad Sci U S A 102(46) (2005) 16830-16835.
[64] Siebold, C., Berrow, N., Walter, T.S., Harlos, K., Owens, R.J., Stuart, D.I., Terman, J.R., Kolodkin, A.L., Pasterkamp, R.J., Jones, E.Y., High-resolution structure of the catalytic region of MICAL (molecule

interacting with CasL), a multidomain flavoenzyme-signaling molecule, Proc Natl Acad Sci U S A 102(46) (2005) 16836-16841.
[65] Entsch, B., Cole, L.J., Ballou, D.P., Protein dynamics and electrostatics in the function of p-hydroxybenzoate hydroxylase, Archives of biochemistry and biophysics 433(1) (2005) 297-311.
[66] Ballou, D.P., Entsch, B., Cole, L.J., Dynamics involved in catalysis by single-component and two-component flavin-dependent aromatic hydroxylases, Biochemical and biophysical research communications 338(1) (2005) 590-598.
[67] Huijbers, M.M., Montersino, S., Westphal, A.H., Tischler, D., van Berkel, W.J., Flavin dependent monooxygenases, Archives of biochemistry and biophysics 544 (2014) 2-17.
[68] Palfey, B.A., McDonald, C.A., Control of catalysis in flavin-dependent monooxygenases, Archives of biochemistry and biophysics 493(1) (2010) 26-36.
[69] Rai, A., Oprisko, A., Campos, J., Fu, Y., Friese, T., Itzen, A., Goody, R.S., Gazdag, E.M., Muller, M.P., bMERB domains are bivalent Rab8 family effectors evolved by gene duplication, eLife 5 (2016).
[70] Hung, R.J., Yazdani, U., Yoon, J., Wu, H., Yang, T., Gupta, N., Huang, Z., van Berkel, W.J., Terman, J.R., Mical links semaphorins to F-actin disassembly, Nature 463(7282) (2010) 823-827.
[71] Hung, R.J., Pak, C.W., Terman, J.R., Direct redox regulation of F-actin assembly and disassembly by Mical, Science 334(6063) (2011) 1710-1713.
[72] Hung, R.J., Spaeth, C.S., Yesilyurt, H.G., Terman, J.R., SelR reverses Mical-mediated oxidation of actin to regulate F-actin dynamics, Nature cell biology 15(12) (2013) 1445-1454.
[73] Grintsevich, E.E., Yesilyurt, H.G., Rich, S.K., Hung, R.J., Terman, J.R., Reisler, E., F-actin dismantling through a redox-driven synergy between Mical and cofilin, Nature cell biology 18(8) (2016) 876-885.
[74] Wu, H., Hung, R.J., Terman, J.R., A simple and efficient method for generating high-quality recombinant Mical enzyme for in vitro assays, Protein expression and purification 127 (2016) 116-124.
[75] Lee, B.C., Peterfi, Z., Hoffmann, F.W., Moore, R.E., Kaya, A., Avanesov, A., Tarrago, L., Zhou, Y., Weerapana, E., Fomenko, D.E., Hoffmann, P.R., Gladyshev, V.N., MsrB1 and MICALs regulate actin assembly and macrophage function via reversible stereoselective methionine oxidation, Molecular cell 51(3) (2013) 397-404.
[76] Alqassim, S.S., Urquiza, M., Borgnia, E., Nagib, M., Amzel, L.M., Bianchet, M.A., Modulation of MICAL Monooxygenase Activity by its Calponin Homology Domain: Structural and Mechanistic Insights, Scientific reports 6 (2016) 22176.
[77] McDonald, C.A., Liu, Y.Y., Palfey, B.A., Actin stimulates reduction of the MICAL-2 monooxygenase domain, Biochemistry 52(35) (2013) 6076-6084.
[78] Zucchini, D., Caprini, G., Pasterkamp, R.J., Tedeschi, G., Vanoni, M.A., Kinetic and spectroscopic characterization of the putative monooxygenase domain of human MICAL-1, Archives of biochemistry and biophysics 515(1-2) (2011) 1-13.
[79] Vitali, T., Maffioli, E., Tedeschi, G., Vanoni, M.A., Properties and catalytic activities of MICAL1, the flavoenzyme involved in cytoskeleton dynamics, and modulation by its CH, LIM and C-terminal domains, Archives of biochemistry and biophysics 593 (2016) 24-37.
[80] Aliverti, A., Curti, B., Vanoni, M.A., Identifying and quantitating FAD and FMN in simple and in iron-sulfur-containing flavoproteins, Methods Mol Biol 131 (1999) 9-23.
[81] Gasteiger, E., Gattiker, A., Hoogland, C., Ivanyi, I., Appel, R.D., Bairoch, A., ExPASy: The proteomics server for in-depth protein knowledge and analysis, Nucleic acids research 31(13) (2003) 3784-3788.
[82] Gill, S.C., von Hippel, P.H., Calculation of protein extinction coefficients from amino acid sequence data, Analytical biochemistry 182(2) (1989) 319-326.
[83] Sun, H., Dai, H., Zhang, J., Jin, X., Xiong, S., Xu, J., Wu, J., Shi, Y., Solution structure of calponin homology domain of Human MICAL-1, Journal of biomolecular NMR 36(4) (2006) 295-300.
[84] Jin, X., Zhang, J., Dai, H., Sun, H., Wang, D., Wu, J., Shi, Y., Investigation of the four cooperative unfolding units existing in the MICAL-1 CH domain, Biophysical chemistry 129(2-3) (2007) 269-278.
[85] Mattevi, A., The PHBH fold: not only flavoenzymes, Biophysical chemistry 70(3) (1998) 217-222.
[86] Schreuder, H.A., Prick, P.A., Wierenga, R.K., Vriend, G., Wilson, K.S., Hol, W.G., Drenth, J., Crystal structure of the p-hydroxybenzoate hydroxylase-substrate complex refined at 1.9 A resolution. Analysis of the enzyme-substrate and enzyme-product complexes, Journal of molecular biology 208(4) (1989) 679-696.

[87] Aliverti, A., Pandini, V., Pennati, A., de Rosa, M., Zanetti, G., Structural and functional diversity of ferredoxin-NADP(+) reductases, Archives of biochemistry and biophysics 474(2) (2008) 283-291.
[88] Gimona, M., Mital, R., The single CH domain of calponin is neither sufficient nor necessary for F-actin binding, Journal of cell science 111 (Pt 13) (1998) 1813-1821.
[89] Gimona, M., Winder, S.J., Single calponin homology domains are not actin-binding domains, Current biology : CB 8(19) (1998) R674-675.
[90] Gimona, M., Djinovic-Carugo, K., Kranewitter, W.J., Winder, S.J., Functional plasticity of CH domains, FEBS letters 513(1) (2002) 98-106.
[91] Galkin, V.E., Orlova, A., Fattoum, A., Walsh, M.P., Egelman, E.H., The CH-domain of calponin does not determine the modes of calponin binding to F-actin, Journal of molecular biology 359(2) (2006) 478-485.
[92] Galkin, V.E., Orlova, A., Salmazo, A., Djinovic-Carugo, K., Egelman, E.H., Opening of tandem calponin homology domains regulates their affinity for F-actin, Nature structural & molecular biology 17(5) (2010) 614-616.
[93] Borrego-Diaz, E., Kerff, F., Lee, S.H., Ferron, F., Li, Y., Dominguez, R., Crystal structure of the actin-binding domain of alpha-actinin 1: evaluating two competing actin-binding models, Journal of structural biology 155(2) (2006) 230-238.
[94] Ribeiro Ede, A., Jr., Pinotsis, N., Ghisleni, A., Salmazo, A., Konarev, P.V., Kostan, J., Sjoblom, B., Schreiner, C., Polyansky, A.A., Gkougkoulia, E.A., Holt, M.R., Aachmann, F.L., Zagrovic, B., Bordignon, E., Pirker, K.F., Svergun, D.I., Gautel, M., Djinovic-Carugo, K., The structure and regulation of human muscle alpha-actinin, Cell 159(6) (2014) 1447-1460.
[95] Tan, X., Thapa, N., Choi, S., Anderson, R.A., Emerging roles of PtdIns(4,5)P2--beyond the plasma membrane, Journal of cell science 128(22) (2015) 4047-4056.
[96] Bach, I., The LIM domain: regulation by association, Mechanisms of development 91(1-2) (2000) 5-17.
[97] Kadrmas, J.L., Beckerle, M.C., The LIM domain: from the cytoskeleton to the nucleus, Nature reviews. Molecular cell biology 5(11) (2004) 920-931.
[98] Nakagawa, H., Suzuki, H., Machida, S., Suzuki, J., Ohashi, K., Jin, M., Miyamoto, S., Terasaki, A.G., Contribution of the LIM domain and nebulin-repeats to the interaction of Lasp-2 with actin filaments and focal adhesions, PloS one 4(10) (2009) e7530.
[99] Koch, B.J., Ryan, J.F., Baxevanis, A.D., The diversification of the LIM superclass at the base of the metazoa increased subcellular complexity and promoted multicellular specialization, PloS one 7(3) (2012) e33261.
[100] Song, Y., DiMaio, F., Wang, R.Y., Kim, D., Miles, C., Brunette, T., Thompson, J., Baker, D., High-resolution comparative modeling with RosettaCM, Structure 21(10) (2013) 1735-1742.
[101] Tuukkanen, A.T., Kleywegt, G.J., Svergun, D.I., Resolution of ab initio shapes determined from small-angle scattering, IUCrJ 3(Pt 6) (2016) 440-447.
[102] Konarev, P.V., Petoukhov, M.V., Svergun, D.I., Rapid automated superposition of shapes and macromolecular models using spherical harmonics, Journal of applied crystallography 49(Pt 3) (2016) 953-960.
[103] Kikhney, A.G., Panjkovich, A., Sokolova, A.V., Svergun, D.I., DARA: a web server for rapid search of structural neighbours using solution small angle X-ray scattering data, Bioinformatics 32(4) (2016) 616-618.
[104] Wijnands, R.A., van der Zee, J., Van Leeuwen, J.W., Van Berkel, W.J., Muller, F., The importance of monopole-monopole and monopole-dipole interactions on the binding of NADPH and NADPH analogues to p-hydroxybenzoate hydroxylase from Pseudomonas fluorescens. Effects of pH and ionic strength, Eur J Biochem 139(3) (1984) 637-644.
[105] Berger, F., Ramirez-Hernandez, M.H., Ziegler, M., The new life of a centenarian: signalling functions of NAD(P), Trends in biochemical sciences 29(3) (2004) 111-118.
[106] Ying, W., NAD+/NADH and NADP+/NADPH in cellular functions and cell death: regulation and biological consequences, Antioxidants & redox signaling 10(2) (2008) 179-206.
[107] Gellert, M., Hanschmann, E.M., Lepka, K., Berndt, C., Lillig, C.H., Redox regulation of cytoskeletal dynamics during differentiation and de-differentiation, Biochimica et biophysica acta 1850(8) (2015) 1575-1587.

[108] Wilson, C., Terman, J.R., Gonzalez-Billault, C., Ahmed, G., Actin filaments-A target for redox regulation, Cytoskeleton (Hoboken) 73(10) (2016) 577-595.
[109] Borquez, D.A., Urrutia, P.J., Wilson, C., van Zundert, B., Nunez, M.T., Gonzalez-Billault, C., Dissecting the role of redox signaling in neuronal development, Journal of neurochemistry 137(4) (2016) 506-517.
[110] Gellert, M., Venz, S., Mitlohner, J., Cott, C., Hanschmann, E.M., Lillig, C.H., Identification of a dithiol-disulfide switch in collapsin response mediator protein 2 (CRMP2) that is toggled in a model of neuronal differentiation, The Journal of biological chemistry 288(49) (2013) 35117-35125.
[111] Galkin, V.E., Orlova, A., Vos, M.R., Schroder, G.F., Egelman, E.H., Near-atomic resolution for one state of f-actin, Structure 23(1) (2015) 173-182.
[112] Takamoto, K., Kamal, J.K., Chance, M.R., Biochemical implications of a three-dimensional model of monomeric actin bound to magnesium-chelated ATP, Structure 15(1) (2007) 39-51.
[113] Manta, B., Gladyshev, V.N., Regulated methionine oxidation by monooxygenases, Free radical biology & medicine (2017).
[114] Oda, T., Iwasa, M., Aihara, T., Maeda, Y., Narita, A., The nature of the globular- to fibrous-actin transition, Nature 457(7228) (2009) 441-445.
[115] Brondani, P.B., Dudek, H.M., Martinoli, C., Mattevi, A., Fraaije, M.W., Finding the switch: turning a baeyer-villiger monooxygenase into a NADPH oxidase, Journal of the American Chemical Society 136(49) (2014) 16966-16969.
[116] Bach, R.D., Mattevi, A., Mechanistic aspects regarding the elimination of H2O2 from C(4a)-hydroperoxyflavin. The role of a proton shuttle required for H2O2 elimination, The Journal of organic chemistry 78(17) (2013) 8585-8593.
[117] McDonald, C.A., Fagan, R.L., Collard, F., Monnier, V.M., Palfey, B.A., Oxygen reactivity in flavoenzymes: context matters, Journal of the American Chemical Society 133(42) (2011) 16809-16811.
[118] Abe, I., Kashiwagi, K., Noguchi, H., Antioxidative galloyl esters as enzyme inhibitors of p-hydroxybenzoate hydroxylase, FEBS letters 483(2-3) (2000) 131-134.
[119] Atkinson-Leadbeater, K., Hehr, C.L., Johnston, J., Bertolesi, G., McFarlane, S., EGCG stabilizes growth cone filopodia and impairs retinal ganglion cell axon guidance, Developmental dynamics : an official publication of the American Association of Anatomists 245(6) (2016) 667-677.
[120] Kaneko, S., Iwanami, A., Nakamura, M., Kishino, A., Kikuchi, K., Shibata, S., Okano, H.J., Ikegami, T., Moriya, A., Konishi, O., Nakayama, C., Kumagai, K., Kimura, T., Sato, Y., Goshima, Y., Taniguchi, M., Ito, M., He, Z., Toyama, Y., Okano, H., A selective Sema3A inhibitor enhances regenerative responses and functional recovery of the injured spinal cord, Nature medicine 12(12) (2006) 1380-1389.
[121] Aggarwal, P.K., Veron, D., Thomas, D.B., Siegel, D., Moeckel, G., Kashgarian, M., Tufro, A., Semaphorin3a promotes advanced diabetic nephropathy, Diabetes 64(5) (2015) 1743-1759.
[122] Chin, M.R., Zlotkowski, K., Han, M., Patel, S., Eliasen, A.M., Axelrod, A., Siegel, D., Expedited access to vinaxanthone and chemically edited derivatives possessing neuronal regenerative effects through ynone coupling reactions, ACS chemical neuroscience 6(4) (2015) 542-550.
[123] Fukuda, M., Kanno, E., Ishibashi, K., Itoh, T., Large scale screening for novel rab effectors reveals unexpected broad Rab binding specificity, Molecular & cellular proteomics : MCP 7(6) (2008) 1031-1042.
[124] Fremont, S., Romet-Lemonne, G., Houdusse, A., Echard, A., Emerging roles of MICAL family proteins - from actin oxidation to membrane trafficking during cytokinesis, Journal of cell science (2017).
[125] Lassing, I., Schmitzberger, F., Bjornstedt, M., Holmgren, A., Nordlund, P., Schutt, C.E., Lindberg, U., Molecular and structural basis for redox regulation of beta-actin, Journal of molecular biology 370(2) (2007) 331-348.
[126] Galkin, V.E., Orlova, A., Cherepanova, O., Lebart, M.C., Egelman, E.H., High-resolution cryo-EM structure of the F-actin-fimbrin/plastin ABD2 complex, Proc Natl Acad Sci U S A 105(5) (2008) 1494-1498.
[127] Kudryashov, D.S., Galkin, V.E., Orlova, A., Phan, M., Egelman, E.H., Reisler, E., Cofilin cross-bridges adjacent actin protomers and replaces part of the longitudinal F-actin interface, Journal of molecular biology 358(3) (2006) 785-797.
[128] Galkin, V.E., Orlova, A., Lukoyanova, N., Wriggers, W., Egelman, E.H., Actin depolymerizing factor stabilizes an existing state of F-actin and can change the tilt of F-actin subunits, The Journal of cell biology 153(1) (2001) 75-86.

[129] Galkin, V.E., Orlova, A., Schroder, G.F., Egelman, E.H., Structural polymorphism in F-actin, Nature structural & molecular biology 17(11) (2010) 1318-1323.
[130] McNicholas, S., Potterton, E., Wilson, K.S., Noble, M.E., Presenting your structures: the CCP4mg molecular-graphics software, Acta crystallographica. Section D, Biological crystallography 67(Pt 4) (2011) 386-394.
[131] Biasini, M., Bienert, S., Waterhouse, A., Arnold, K., Studer, G., Schmidt, T., Kiefer, F., Gallo Cassarino, T., Bertoni, M., Bordoli, L., Schwede, T., SWISS-MODEL: modelling protein tertiary and quaternary structure using evolutionary information, Nucleic acids research 42(Web Server issue) (2014) W252-258.
[132] Fontes, R., Ribeiro, J.M., Sillero, A., Inhibition and activation of enzymes. The effect of a modifier on the reaction rate and on kinetic parameters, Acta biochimica Polonica 47(1) (2000) 233-257.